Energy Economics 149 (2025) 108700

Contents lists available at ScienceDirect

Energy Economics

journal homepage: www.elsevier.com/locate/eneeco

Compounding geopolitical and energy risks: A clustered stochastic multi-COVOL model

Ovielt Baltodano López, Monica Billio *, Roberto Casarin, Michele Costola

Department of Economics, University Ca' Foscari Venezia, Venezia, Italy

ARTICLE INFO

JEL classification:
C51
C58
C38
G11
G15

Keywords:
Compounding risks
Clustered factors
Latent factors
Energy uncertainty
Financial markets
Geopolitical risk
Volatility comovements

ABSTRACT

This paper investigates the relationship between stock returns in the energy sector, energy uncertainty, and geopolitical risk. To this end, we propose a parsimonious and flexible model to extract common volatility factors (COVOL) from panel data. This general nonlinear multi-factor framework organizes panel units into groups based on different exposures to individual and compounding risks to reduce the number of parameters to be estimated. The group membership of the units is unknown, which naturally calls for using stochastic partition models. Random partition and compounding relationships are encoded in the weighted hyper-edges of a random hypergraph where the vertexes are the individual risks. In the empirical analysis, we study the volatility transmission in a multi-country setting and the role of individual and compounding risks.

1. Introduction

Over the last decades, the relationship between energy markets and geopolitical events has increased, with shocks to energy prices potentially reshaping long-term energy policies. Examples of this phenomenon in the oil market include the 1973 embargo imposed by OAPEC against nations that supported Israel during the Yom Kippur War and the 1980–81 Iran–Iraq war (Hamilton, 1983).

Europe's dependence on Russian gas, a key energy source, has highlighted its vulnerability to geopolitical tensions. This weakness in energy provision was evident during the gas disputes between Ukraine and Russia in 2006 and 2009, which caused notable supply interruptions. Costola and Lorusso (2022) find that Russian geopolitical uncertainty affected energy commodity volatility, with the oil and gas industry experiencing spillover effects during Ukraine-related disputes in Crimea and subsequent trade restrictions. The escalation reached its height in 2022 when Russia invaded Ukraine, leading to unprecedented international sanctions against Russia (Egorov, 2023), which provoked spikes in energy prices and increased market volatility. Natural gas prices hit an all-time high in August 2022 at the Title Transfer Facility in Amsterdam, a central European trading hub. Consequently, European countries searched for alternative energy providers, diversified their sources, and lessened their dependence on a single supplier. Geopolitical risks can have indirect consequences, propagating volatility in energy markets and affecting stock markets. Smales (2021) finds that such risks impact both oil and stock market volatility, with a more pronounced impact on oil prices and spillover effects from oil to stock returns.

To assess geopolitical risk (GPR), Caldara and Iacoviello (2022) proposed an index that uses newspaper articles for measuring geopolitical tensions at the country or global level, similar to how (Baker et al., 2016) gauge economic policy uncertainty. The authors, along with several subsequent studies (Liu et al., 2019; Wang et al., 2019; Baur and Smales, 2020; Gong and Xu, 2022), have shown that the GPR index provides informative signals at both the macro and micro levels across various markets. In this respect, scholars and practitioners presented different types of uncertainty and risk indicators to track particular categories of events that might affect economic growth and

* Corresponding author.
E-mail addresses: ovielt.baltodano@unive.it (O. Baltodano López), billio@unive.it (M. Billio), r.casarin@unive.it (R. Casarin), michele.costola@unive.it (M. Costola).

https://doi.org/10.1016/j.eneco.2025.108700
Received 31 July 2024; Received in revised form 19 June 2025; Accepted 22 June 2025
Available online 28 July 2025

financial stability (see, for instance, policyuncertainty.com, the central hub collector originated after the work of Baker et al., 2016).

All these indices represent distinct and separate sources of uncertainties and risks.[1] In the context of financial markets, Engle and Campos-Martins (2023) have recently proposed a GARCH multivariate model that uses a multiplicative decomposition of the cross-section of innovations to capture common variations in volatility (COVOL). Findings on COVOL revealed the presence of global effects during periods of geopolitical tensions and international crises such as the COVID-19 pandemic.

The presence of concurrent hazard situations, each with unique underlying features, can create compounding vulnerabilities that result in a non-linear increase in total exposure, exceeding the sum of the individual components (Billio and Varotto, 2020; Kruczkiewicz et al., 2021; Dunz et al., 2023). This motivates us to consider alternative sources of risk and uncertainty that might lead to common volatility changes, with different groups of assets having varying levels of exposure to these factors. Building on the work of Engle and Campos-Martins (2023), we extend the canonical COVOL model to incorporate multiple latent factors that account for alternative individual and joint sources of uncertainty and risk arising from energy stock markets, geopolitical risk, and energy uncertainty.

Specifying a full variance–covariance structure to identify compound risks is a complex task involving many parameters. We exploit the COVOL framework to capture the dependence between the risks across countries and extend it to account for model parsimony, compounding risks, and COVOL persistence. Our econometric contribution is manifold.

First, we assume the covolatility factor (COVOL) follows a latent gamma autoregressive process, thus contributing to the gamma model literature (e.g., see Engle and Russell, 1998; Engle, 2002; Engle and Gallo, 2006; Gouriéroux and Jasiak, 2006; Creal et al., 2013; Alitab et al., 2019; Bormetti et al., 2020). The dynamic specification of the stochastic COVOL captures persistence and comovement clustering effects. It allows us to derive some important theoretical properties of the model. We show persistence provides essential information on shock propagation and lagged spill-over effects. Second, a random hypergraph is assumed to drive the potential risk interactions in a multi-factor extension of the canonical COVOL model (Engle and Campos-Martins, 2023). The hypergraph allows for a simple representation of the model and for identifying the different compounding degrees of the risks. The use of the COVOL specification in our new factor model provides a contribution to the literature on factor models (e.g., see Yamauchi and Omori, 2023; Gregor Kastner and Lopes, 2017; Bai and Ng, 2006; Han, 2006; Aguilar and West, 2000), and the use of restrictions encoded by a random hypergraph contributes to the graphical model literature (e.g., see Ahelegbey et al., 2016a, 2024, 2016b; Agudze et al., 2022). Finally, a Bayesian inference framework with hierarchical priors and clustering effects allows for a parsimonious model for cross-sectional heterogeneity in risk exposures. We assume the panel units are partitioned into distinct, non-overlapping groups. Both observable and latent partitions drive the clustering effects. The new clustered COVOL model provides a contribution to the literature on cross-sectional clustering in panel data models (e.g., see Hirano, 2002; Bauwens and Rombouts, 2007; Billio et al., 2019; Fisher and Jensen, 2022; Casarin et al., 2024).

We apply our clustered stochastic COVOL model to analyze the relationship between the energy stock market, energy uncertainty, and geopolitical risk. We investigate the co-movements in the fluctuations of a multi-country panel of uncertainty measures and geopolitical risk measures that may impact the global energy sector. Fig. 1 shows the pairwise correlations between variables of a panel of countries. The series squares have been used as a proxy of the second moment of the variables, and a stochastic-block model algorithm has been applied to identify groups of countries and blocks in the correlation matrix (dashed lines).[2] The preliminary analysis evidenced the presence of clustering effects in the dependence between the energy sector fluctuations (top-left plot). Similar effects appear in the dependence between energy uncertainty (top-right plot) and geopolitical risk fluctuations (bottom plot). For all pairs of countries, the significant correlations are positive. Another important stylized fact is the co-movement persistence, reported in previous studies (Engle and Campos-Martins, 2023; Campos-Martins and Hendry, 2024). This paper provides a new, flexible model with multiple stochastic COVOL factors to capture clustering effects and persistence.

The paper is organized as follows. Section 2 presents the clustered stochastic multi-factor COVOL model and its properties, together with some possible extensions or alternative specifications. Section 3 presents a Bayesian likelihood-based inference, the posterior approximation method and discusses its efficiency based on simulation experiments. Section 4 presents the main empirical findings on the relationship between uncertainty and risk volatility and the energy sector volatility. Section 5 concludes.

2. A stochastic comovement model

We present the model with a common stochastic volatility factor, COVOL, and cross-section clustering effects. Some relevant properties of the model are discussed, and the proofs of the results of this section are given in Appendix B. Then, this model is extended to account for compounding risks by proposing a multi-factor setting using a random hypergraph, where the hypernodes represent the type of risks, the hyperedges their interactions, and the hyper-weights the exposure to individual and compounding risks.

2.1. Co-movements persistence

The returns of N financial assets satisfy the following equation

$$r_{it} = \sqrt{g_i(x_t)}\varepsilon_{it}, \quad \varepsilon_{it} \sim \mathcal{N}(0,1), \tag{1}$$

$t = 1, \ldots, T$, $i = 1, \ldots, N$, where x_t is a common volatility risk factor (COVOL), ε_{it} are i.i.d. Gaussian innovation terms and $g_i(\cdot)$ is skedastic function mapping from the common factor space $\mathbb{R}_+$ to the ith asset volatility space $\mathbb{R}_+$.

To capture the persistence in the COVOL, we assume the COVOL follows an Autoregressive Gamma process (Gouriéroux and Jasiak, 2006) of the first order (ARG)

$$x_t | x_{t-1} \sim \mathcal{G}^*(\alpha_t(\theta), \beta_t(\theta)x_{t-1}, \tau_t(\theta)) \tag{2}$$

$t = 1, 2, \ldots$, where $\mathcal{G}^*(a, b, c)$ denotes the non-central gamma distribution with shape, non-centrality, and scale parameters $a > 0$, $b > 0$ and $c > 0$, respectively. For the constant parameter case, $\alpha_t(\theta) = a$, $\beta_t(\theta) = b$ and $\tau_t(\theta) = c$, from the stationarity condition $cb < 1$, it follows that the unconditional mean and variance of this process are given by $\mathbb{E}(x_t) = ca/(1 - cb)$ and $\mathbb{V}(x_t) = ac^2/(1 - cb)^2$.

[1] It is important to note that, in principle, risk refers to situations with known probabilities of outcomes, allowing for quantification and management, while uncertainty involves situations where these probabilities are unknown, making outcomes unpredictable and more challenging to manage (Knight, 1921; Epstein and Wang, 2004).

[2] Stochastics block models (SBM) cluster the set of assets with similar correlation structures as nodes in a weighted and undirected network with similar connectivity parameters. The estimation of the SBM uses a Variational-EM algorithm, and the number of clusters is selected using the Integrated Complete likelihood (ICL) (Mariadassou et al., 2010; Biernacki et al., 2000). The R package by Leger (2016) is used for the computations presented in the preliminary analysis in Fig. 1.

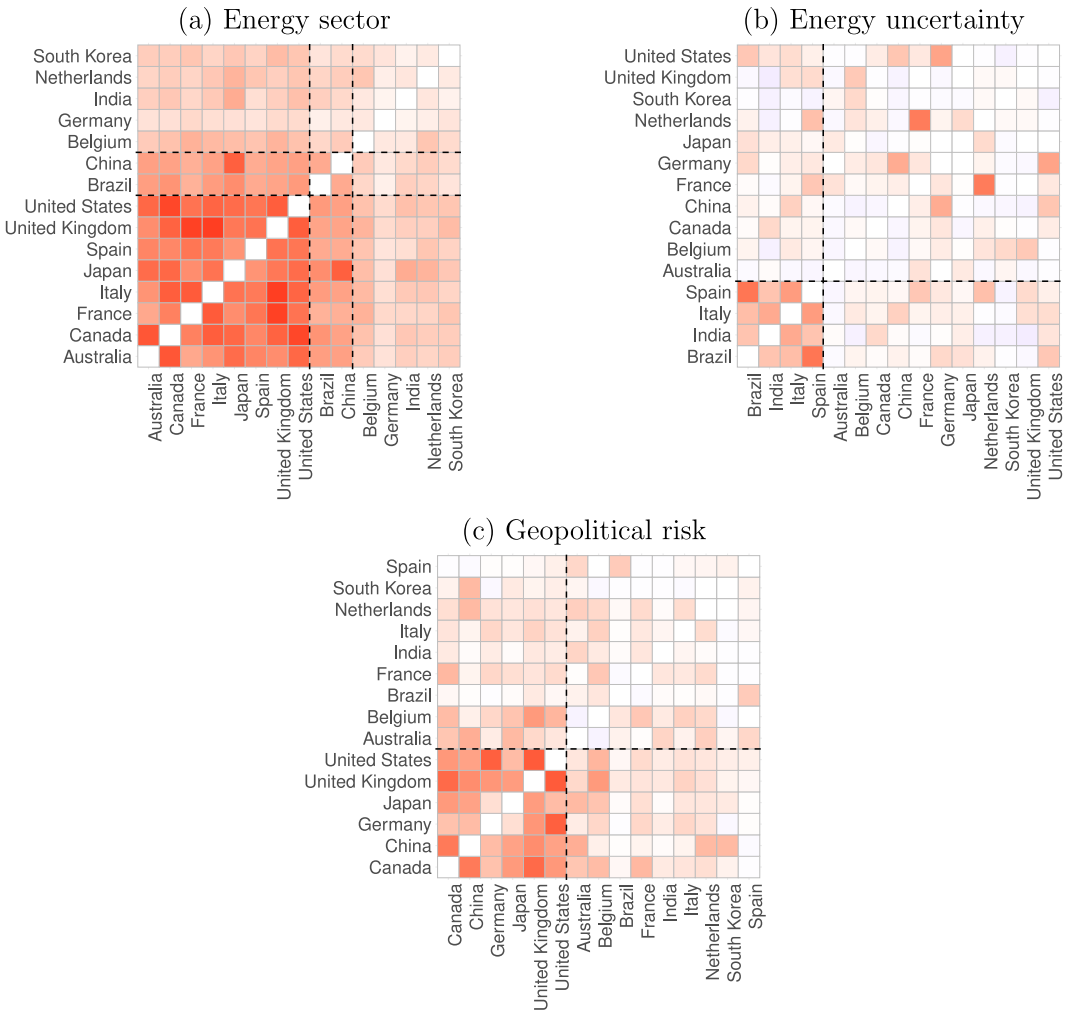

Fig. 1. In each plot, the pairwise correlations between the squared values of the time series from different countries (rows and columns) are displayed. Red (■) and blue (■) shades represent the spectrum from high positive to weak negative correlation values, while white (□) cells indicate null correlations. Dashed lines identify the correlation blocks extracted with a stochastic block algorithm.

Consistently with Campos-Martins and Hendry (2024), this paper further assumes the parameters of the common volatility process are driven by a random scale process $\upsilon_t > 0$, $t = 1, \dots, T$, that is $\theta = (\widetilde{\alpha}, \rho)'$ with $\alpha_t(\theta) = 1/\upsilon_t$, $\beta_t(\theta) = \rho/(\widetilde{\alpha}\upsilon_t)$ and $\tau_t(\theta) = (1-\rho)\upsilon_t$. The parameter $\widetilde{\alpha} \in (0, 1)$ is the scaled degrees of freedom, and $\rho \in (0, 1)$ is the persistence parameter such that stationary and unit mean conditions are satisfied, i.e. $\widetilde{\alpha} + \rho = 1$. The sequence υ_t, $t = 1, \dots, T$ is an independent Gamma process

$$\upsilon_t \sim \mathcal{G}(d, 1/d), \tag{3}$$

where $\mathcal{G}(a', b')$ denotes a Gamma distribution with shape and rate parameters, $a' > 0$ and $b' > 0$. Note that $\mathcal{G}(a', b')$ can be obtained from $\mathcal{G}^*(a, b, c)$ as $b \to 0$, $a = a'$ and $c = 1/b'$.

Our model for the common factor allows for persistence and, under the stationarity and unit mean conditions, presents properties consistent with the ones of the model in Engle and Campos-Martins (2023). Compared to the standard ARG model in Gouriéroux and Jasiak (2006), our common factor exhibits a stochastic scale. Some properties of this process are presented below.

Proposition 1 (*Common Factor Properties*). *Let $\mathcal{F}_t^{\upsilon} = \sigma(\upsilon_1, \dots, \upsilon_t)$ be the σ-field generated by the past values of the random volatility process υ_t. The common factor $x_t > 0$, $t = 1, \dots, T$ satisfies*

1. $\mathbb{E}(x_t) = \mathbb{E}(x_t|\mathcal{F}_t^{\upsilon}) = 1$;
2. $\mathbb{V}(x_t|\mathcal{F}_t^{\upsilon}) = (1-\rho^2)\sum_{i=0}^{t-1}\rho^{2i}\upsilon_{t-i}$; $\mathbb{V}(x_t) = d^2$;
3. $\mathbb{C}ov(x_t, x_{t-h}|\mathcal{F}_t^{\upsilon}) = \rho^h(1-\rho^2)\sum_{i=0}^{t-h-1}\rho^{2i}\upsilon_{t-i}$; $\mathbb{C}ov(x_t, x_{t-h}) = \rho^h d^2$.

If the common factor is not persistent, $\rho = 0$, then one recovers from Proposition 1 the model given in Engle and Campos-Martins (2023). In the case of non-explosive persistence, $0 < \rho < 1$, the COVOL follows a covariance-stationary process, i.e. constant mean and variance and decaying autocorrelation depending only on the horizon h.

The choice of the skedastic function is crucial to recover the desired model properties. An essential requirement is to keep a unit variance for r_{it} to separate the unit-specific dynamic of the variances and the dependence in the second moment between assets. In this sense, we assume the asset volatility depends linearly on the common factor x_t as in Campos-Martins and Hendry (2024) and Engle and Campos-Martins (2023). However, the number of factor loadings increases with the number of assets. To deal with overparametrization, we follow a Bayesian inference approach and use a hierarchical prior distribution for the factor loadings to achieve parameter parsimony. Our prior combines parameter clustering and shrinking effects. At the first stage of the hierarchical prior, we introduce the following clustering mechanism in the skedastic function:

$$g_i(x_t) = g(x_t, z_i) = s(z_i)x_t + 1 - s(z_i), \quad s(z_i) = \sum_{k=1}^{K}\mathbb{I}(z_i \in \{k\})\lambda_k \tag{4}$$

with $\lambda_k \in [0, 1]$ a common factor loading coefficient. The membership variable z_i assigns the ith asset to a specific group with probability

$\mathbb{P}(z_i = k) = \pi_k$. The clustering effect is a desirable feature for the model since groups of assets can have similar volatility features and exposure to the common volatility factor, following the evidence in previous studies (Fisher and Jensen, 2022; Casarin et al., 2024). For $K = n$ and $z_i = i$ one gets the scale factor as in Engle and Campos-Martins (2023), that is $g_i(x_t) = \lambda_i x_t + 1 - \lambda_i$.

Regarding the second stage of the hierarchical prior, the following hyper-priors can be assumed further $(\pi_1, \dots, \pi_K)' \sim \mathcal{D}(1/K, \dots, 1/K)$, which corresponds to a Dirichlet distribution with $[1/K, \dots, 1/K]'$ as concentration hyper-parameters and standard uniform for the exposure λ_k. Alternative specification of the hierarchical prior can be used. At the first stage, one can assume a prior which guarantees that the loadings belong to the unit interval and have a unit norm for identification purposes, such as a Dirichlet prior $(\lambda_1, \dots, \lambda_N)'|\xi \sim \mathcal{D}(\xi_1, \dots, \xi_N)$. In the second stage, a mixture prior allowing for cross-sectional clustering and shrinking towards a common mean can be used, such as the multinoulli distribution $\xi_i \sim \sum_{k=1}^{K} \pi_k m_k$. The specification of the Bayesian model is completed with the assumption of a normal prior for the logit transformation of ρ to guarantee the covariance-stationarity of the Gamma autoregressive process ($0 < \rho < 1$), and of a gamma prior on d.

Under the specification in Eqs. (1)–(4) and the weak stationarity assumption, the model has the following properties, which are helpful for model interpretation and posterior predictive checking. While there is no correlation between the levels of returns, the covariance between squared returns presents a block structure clustered by membership interactions, and a similar effect applies to the variances. As stated in the following, the parameter of the stochastic scale v_t and the loadings λ_k determine the behavior of the fourth-order moments of r_{it}.

Proposition 2 (*Conditional Model Properties given the Membership*)**.** *Let $\mathcal{F}_t^r = \sigma(\mathbf{r}_1, \dots, \mathbf{r}_t)$ be the σ-field generated by the return vector process $\mathbf{r}_t$ $t = 1, 2, \dots$, and $\mathcal{F}_{t-1} = \mathcal{F}_{t-1}^r \vee \mathcal{F}_t^v$ the augmented σ-field. The return process r_{it} $i = 1, \dots, N$ satisfies*

1. $\mathbb{E}(r_{it}|\mathcal{F}_{t-1}^r \vee \{z_i = k\}) = 0$ *and* $\mathbb{V}(r_{it}|z_i = k) = 1$;
2. $\mathbb{C}ov(r_{it}, r_{jt}|\mathcal{F}_{t-1}^r \vee \{z_i = k, z_j = \ell\}) = 0$ *for* $i \neq j$;
3. $\mathbb{V}(r_{it}^2|z_i = k) = 3\lambda_k^2 d^2 + 2$;
4. $\mathbb{C}ov(r_{it}^2, r_{jt}^2|z_i = k, z_j = \ell) = d^2 \lambda_k \lambda_\ell$ *for* $i \neq j$.

This extends the result of Engle and Campos-Martins (2023), allowing for cross-sectional clustering effects. For a given number of K groups of assets, the exposure level to the stochastic COVOL varies and is constant within each group.

Also, our ARG model assumption captures possible persistence in the comovements. Given the past values of v_t, the persistence in the ARG leads to time-varying covariances and autocovariances, as stated in the following two propositions.

Proposition 3 (*Other Conditional Model Properties*)**.** *The return process $\mathbf{r}_t$, $t = 1, 2, \dots$, $i = 1, \dots, N$ satisfies*

1. $\mathbb{E}(r_{it}|\mathcal{F}_t) = 0$ *and* $\mathbb{V}(r_{it}|\mathcal{F}_t^v) = 1$;
2. $\mathbb{C}ov(r_{it}, r_{jt}|\mathcal{F}_t) = 0$ *for* $i \neq j$;
3. $\mathbb{V}(r_{it}^2|\mathcal{F}_t^v) = 3((1-\rho^2)\sum_{s=0}^{t-1} \rho^{2s} v_{t-s})(\sum_k \sum_\ell \pi_k \pi_\ell \lambda_k \lambda_\ell) + 2$;
4. $\mathbb{C}ov(r_{it}^2, r_{jt}^2|\mathcal{F}_t^v) = [(1-\rho^2)\sum_{s=0}^{t-1} \rho^{2s} v_{t-s}] \sum_{k=1}^{K} \sum_{\ell=1}^{K} \lambda_k \lambda_\ell \pi_k \pi_\ell$ *for* $i \neq j$.

The persistence parameter determines the dynamic feature of the factor, as illustrated in Fig. 2. The top left plot shows that larger values of the persistence parameter ρ (solid and dashed lines) are associated with slower convergence to the equilibrium of the conditional variance of the squared variable r_{it}^2, compared to the low persistence case (dotted lines and dashed–dotted lines). Large persistence also implies a higher autocorrelation level of the process (right plot, solid line).

The bottom plot illustrates the effects of the autoregressive coefficient ρ and the factor loadings λ_k on the cross-autocovariance. If two series are in two groups with high and low exposures to a highly persistent factor (solid line), then the level of cross-autocovariance will be larger than in the case of the two series belonging to groups with low exposures to a common highly persistent factor (dashed line) or a common low persistent factor (dotted and dashed–dotted lines). The analytical value of the cross-autocovariance is given below.

Proposition 4 (*Dynamic Properties*)**.** *The return processes $\mathbf{r}_t$ $t = 1, 2, \dots$, $i = 1, \dots, N$ satisfy*

1. $\mathbb{C}ov(r_{it}^2, r_{jt-h}^2|\mathcal{F}_t^v) = \rho^h(1-\rho^2)(\sum_{s=0}^{t-h-1} \rho^{2s} v_{t-s})(\sum_k \sum_\ell \pi_k \pi_\ell \lambda_k \lambda_\ell)$ $\forall$ $i, j \in \{1, \dots, N\}$;
2. $\mathbb{C}ov(r_{it}^2, r_{it-h}^2) = \mathbb{C}ov(r_{it}^2, r_{jt-h}^2) = \rho^h d^2 \sum_k \sum_\ell \pi_k \pi_\ell \lambda_k \lambda_\ell$ *for* $i \neq j$;
3. $\mathbb{C}ov(r_{it}^2, r_{it-h}^2|z_i = k) = \rho^h d^2 \lambda_k^2$ *and* $\mathbb{C}ov(r_{it}^2, r_{jt-h}^2|z_i = k, z_j = \ell) = \rho^h d^2 \lambda_k \lambda_\ell$ *for* $i \neq j$.

Finally, the unconditional moments of the squared processes incorporate the uncertainty in the membership and scaling while keeping the same properties for the returns in levels. For further details, see Appendix B.

Proposition 5 (*Unconditional Model Properties*)**.** *The return processes $\mathbf{r}_t$ $t = 1, 2, \dots$, $i = 1, \dots, N$ satisfy*

1. $\mathbb{E}(r_{it}) = 0$ *and* $\mathbb{V}(r_{it}) = 1$;
2. $\mathbb{C}ov(r_{it}, r_{jt}) = 0$ *for* $i \neq j$;
3. $\mathbb{V}(r_{it}^2) = 3d^2(\sum_k \sum_\ell \pi_k \pi_\ell \lambda_k \lambda_\ell) + 2$;
4. $\mathbb{C}ov(r_{it}^2, r_{jt}^2) = d^2 \sum_{k=1}^{K} \sum_{\ell=1}^{K} \lambda_k \lambda_\ell \pi_k \pi_\ell$ *for* $i \neq j$.

Following the same proof strategies, similar model properties can be derived for the alternative prior specifications discussed above (see Appendix A).

2.2. Asset partition

Regarding the cross-sectional grouping, there are many alternative specifications. In this paper, we combine two strategies. In the first strategy, the partition with elements $\mathcal{D}_1, \dots, \mathcal{D}_K$ such that $\mathcal{D}_k \cap \mathcal{D}_\ell = \emptyset$ for $k \neq \ell$, is not observed and can be determined on a statistical basis.

A second strategy exploits the exogenous partition of the N assets into groups based on available information such as economic sectors, type of assets, and type of variables. In this specification the cross-section $\{1, \dots, N\}$ is partitioned into $\mathcal{D}_1, \dots, \mathcal{D}_M$ such that $\mathcal{D}_q \cap \mathcal{D}_w = \emptyset$ for $q \neq w$, where M is the number of groups. In the COVOL specification of the previous section, $M = 1$.

A third, more general specification composes the first and second partition strategies. This is achieved by assuming that each exogenously given group $\mathcal{D}_q$ comprises K unobserved groups $\mathcal{D}_{kq}$ with $k = 1, \dots, K$ and $q = 1, \dots, M$, resulting in a total of KM clusters.

2.3. Multiple COVOL factors

For each unit i in the panel, we assume J variables are available r_{ijt}, $j = 1, \dots, J$, which satisfies the following set of equations

$$r_{ijt} = \sqrt{g_{ij}(\boldsymbol{x}_t)}\epsilon_{ijt}, \quad \epsilon_{ijt} \sim \mathcal{N}(0, 1), \tag{5}$$

$t = 1, \dots, T$, $i = 1, \dots, N$, $j = 1, \dots, J$, where $\boldsymbol{x}_t \in \mathbb{R}_+^p$ is a vector of COVOL factors, ϵ_{ijt} are i.i.d. Gaussian innovation terms and $g_{ij}(\cdot)$ is a skedastic function mapping from the common factor space $\mathbb{R}_+^p$ to the ith unit volatility space $\mathbb{R}_+$ in the variable j, where p is the number of factors.

Let $\mathcal{M} = \{1, \dots, M\}$ be the set of all risks considered in the compounding, with $M \leq J$. The potential number of COVOL factors is $p = 2^M - 1$. As proposed in the previous section, to deal with overparametrization in a large-factor model, we introduce the observed clustering indicator $c_j \in \mathcal{M}$ and the unobserved clustering indicator

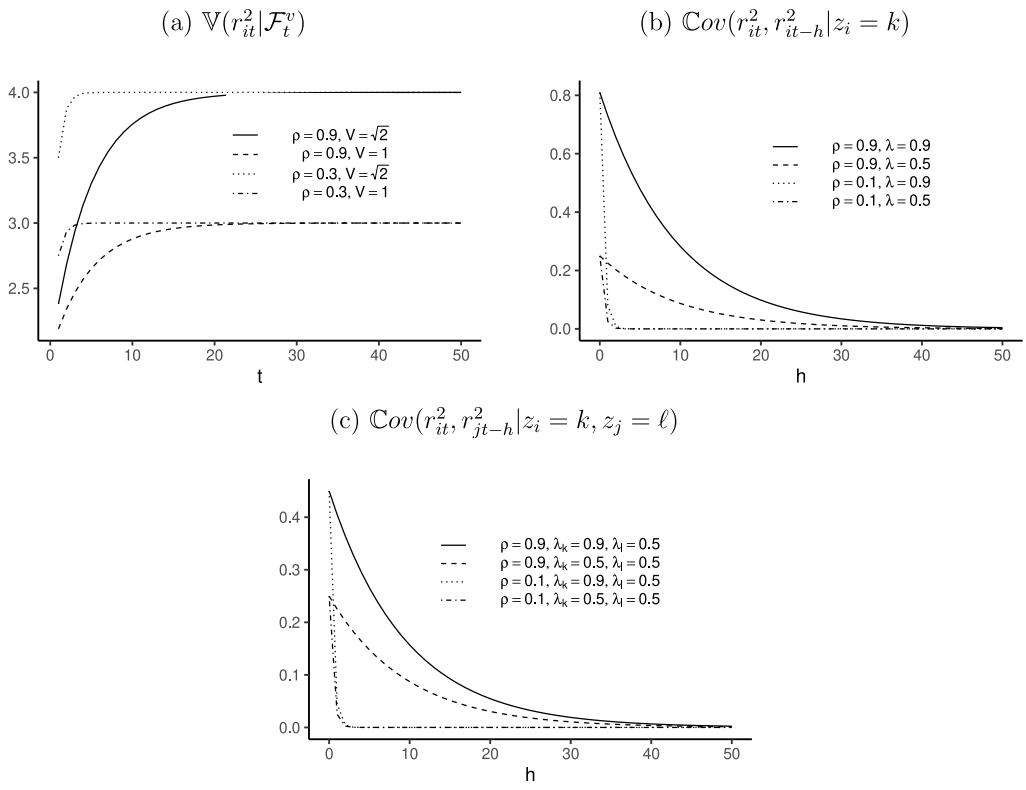

Fig. 2. Conditional model properties for different parameter settings (different lines).

$z_{qi} \in \{1, \dots, K\}$ for $q \in \mathcal{M}$. We further assume the risk composition is given by a set of restrictions on the factor loadings, which can be represented by an undirected hypergraph $\mathcal{G} = (\mathcal{V}, \mathcal{E})$, where the ordered pair includes the set of nodes $\mathcal{V}$, given by the different type of risks $\mathcal{V} = \mathcal{M}$ and the hyperedge set $\mathcal{E} = \bigcup_{i=1}^{N} \bigcup_{j=1}^{J} \mathcal{E}_{ij}$ with $\mathcal{E}_{ij} = \{e_{ij1}, \dots, e_{ijH_{ij}}\}$ and $e_{ij\ell} \subseteq \mathcal{M}$ where H_{ij} indicates the number of relevant relationships between the risks.

In our model, self-loops are allowed in the hyperedges to represent the absence of risk compounding (zero-degree compounding). The higher the cardinality of a hyperedge $e_{ij\ell}$, the higher the number of risks involved in the compounding, i.e. the degree of compounding is $|e_{ij\ell}| - 1$. The structure of risk compounding effects is the same for all units, that is, $\mathcal{E}_{ij} = \mathcal{E}_j$, but their strength may differ as explained in the following.

The skedastic function with multiple COVOL factors allows for different degrees of risk compounding effects

$$g_{ij}(\boldsymbol{x}_t) = g(\boldsymbol{x}_t, c_j, z_{c_j i}) = \sum_{\mathcal{U} \in \mathcal{E}} \mathbb{I}(c_j \in \mathcal{U}) s_{j(\mathcal{U})}(z_{c_j i}) x_{(\mathcal{U})t} + \tilde{s}_j(z_{c_j i}) \tag{6}$$

with $\tilde{s}_j(z_{c_j i}) = 1 - \sum_{\mathcal{U} \in \mathcal{E}} \mathbb{I}(c_j \in \mathcal{U}) s_{j(\mathcal{U})}(z_{c_j i}) \in (0, 1)$ and $\boldsymbol{x}_t = \{x_{(\mathcal{U})t}\}_{\mathcal{U} \in \mathcal{E}}$. The exposures $s_{j(\mathcal{U})}(z_{c_j i})$ indicate the relevance of a specific compounding risk for each unit i and variable j. They can be interpreted as the hyperweights $\mathcal{W} = \{w_{ij}\}_{ij}$, $w_{ij}(\mathcal{U}) = s_{j(\mathcal{U})}(z_{c_j i})$, $\mathcal{U} \in \mathcal{E}$ which measure the strength of the hyperedges in the hypergraph $\mathcal{G} = (\mathcal{V}, \mathcal{E}, \mathcal{W})$

The unobserved clustering induced by z_{qi} reduces further the number of loadings to estimate from NJp to $KJ|\mathcal{E}_j|$ through the prior assumption

$$s_{j(\mathcal{U})}(z_{c_j i}) = \sum_{k=1}^{K} \mathbb{I}(z_{c_j i} = k) \lambda_{j(\mathcal{U})k},$$

with $\pi(z_{qi} = k) = \pi_q$, where the edge $\mathcal{U}$ belongs to the hyperedge set $\mathcal{E}_j$ and represents the set of risks being compounded. The common volatility factors follow the ARG process described in (2)

$$x_{(\mathcal{U})t} | x_{(\mathcal{U})t-1} \sim \mathcal{G}^*(1/v_{(\mathcal{U})t}, \rho_{(\mathcal{U})}/((1 - \rho_{(\mathcal{U})})v_{(\mathcal{U})t})x_{(\mathcal{U})t-1}, (1 - \rho_{(\mathcal{U})})v_{(\mathcal{U})t}). \tag{7}$$

Some examples of this general model specification are presented in the following for $M = J = 3$ and in Fig. 3.

Example 2.1 (*Absence of Compounding*)**.** In zero-degree compounding, only individual risks are considered. The exogenous clustering corresponds to the variable type, $c_j = j$, $\mathcal{U} = \{q\}$ and $j(q) = j$, and there is no interaction between the different types of risks

$$g_{ij}(x_t) = \sum_{q=1}^{M} \mathbb{I}(c_j = q) s_{j(q)}(z_{c_j i}) x_{(q)t} + \tilde{s}_j(z_{c_j i}) = s_j(z_{ji}) x_{jt} + (1 - s_j(z_{ji})).$$

The last expression coincides with the one in Eq. (4) when only one variable per unit is considered (i.e. $J = 1$). In our application, where three variables are used, $J = 3$, $\mathcal{M} = \{1, 2, 3\}$ corresponds to $\{EMI, EUI, GPR\}$ and the hyperedge set becomes $\mathcal{E} = \{\{1\}, \{2\}, \{3\}\}$. Since two unobserved groups are assumed, $K = 2$, the constraint $\lambda_{j(q)1} > \lambda_{j(q)2}$ for $q = 1, 2, 3$ implies that the units are clustered into high and low exposure to each risk source, and a total of $MK = 6$ clusters are considered. A graphical illustration is given in panel a) of Fig. 3.

Example 2.2 (*Global Compounding*)**.** If individual risk COVOLs are not included and only a (second-degree) global compounding risk is considered, then the edge set is $\mathcal{E} = \{\{1, 2, 3\}\}$ and the skedastic function becomes

$$g_{ij}(x_t) = s_{j(123)}(z_{c_j i}) x_{(123)t} + \tilde{s}_j(z_{c_j i}).$$

As in the previous example, six clusters can be used to divide units between high and low exposure to the second-degree compounding risk, $\lambda_{j(123)1} > \lambda_{j(123)2}$ A graphical illustration is given in panel b) of Fig. 3.

Example 2.3 (*Conditional Global Compounding*)**.** When both individual risk COVOLs (zero-degree compounding) and a compounding risk COVOL (second-degree compounding) are assumed, the skedastic function

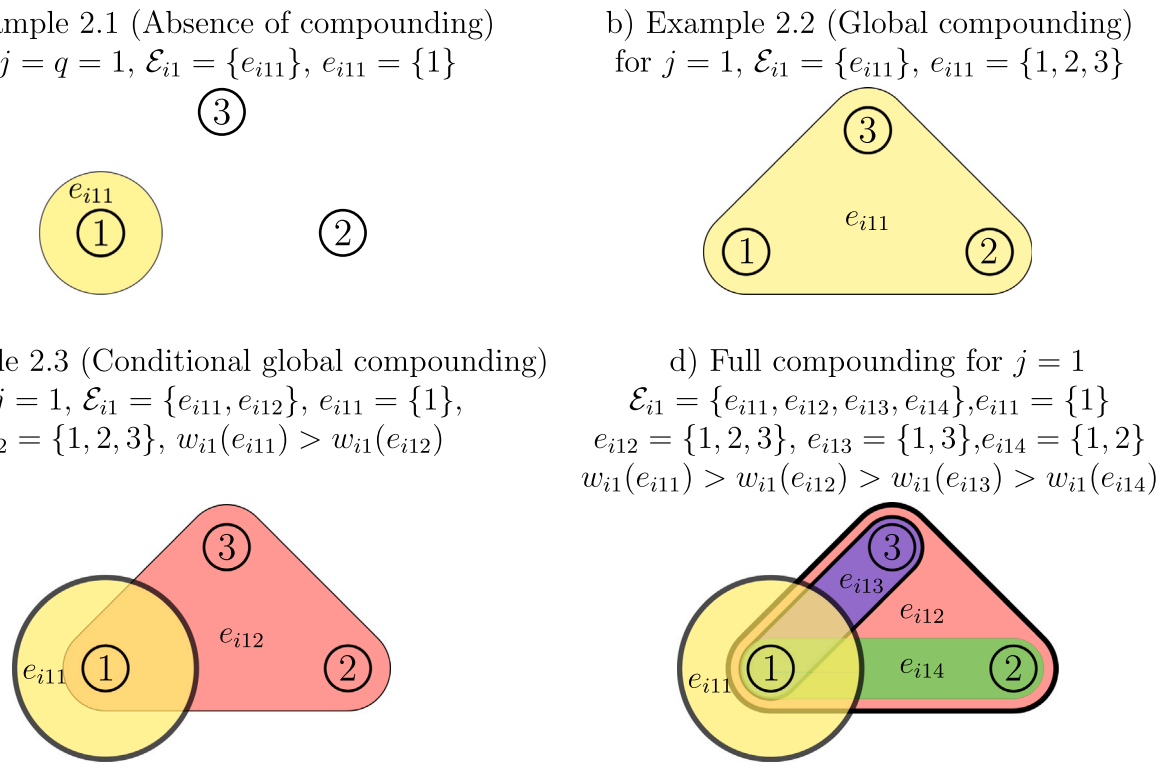

Fig. 3. Hypergraph representation of compounding risks for $\mathcal{G}_{ij}$, the node 1 refers to the EMI risk, node 2 to the EUI risk and node 3 to the GPR risk. The colored shapes represent the hyperedges and the line width the hyperweights equivalent to the exposures for unit i. (For interpretation of the references to color in this figure legend, the reader is referred to the web version of this article.)

becomes

$$g_{ij}(x_t) = \sum_{q=1}^{M} \mathbb{I}(c_j = q) s_{j(q)}(z_{c_j i}) x_{(q)t} + s_{(123)}(z_{c_j i}) x_{(123)t} + \tilde{s}_j(z_{c_j i}).$$

Similarly, the number of clusters per variable is $K = 2$, which corresponds to high and low exposure to second-degree compounding risk, i.e. $\lambda_{j(123)1} > \lambda_{j(123)2}$. The total number of clusters is $MK = 6$. A graphical illustration is given in panel c) of Fig. 3.

Example 2.4 (*Full Compounding*)**.** In the full compounding all degrees of risk composition appear in the skedastic function, which can be written by grouping hyperedges $\mathcal{U}$ following their cardinality from 1 (zero-degree) to M ($M - 1$ degree)

$$\begin{aligned} g_{ij}(\boldsymbol{x}_t) = g(\boldsymbol{x}_t, c_j, z_{c_j i}) = \\ \underbrace{\sum_{q=1}^{M} \mathbb{I}(c_j \in \{q\}) s_{j(q)}(z_{c_j i}) x_{(q)t}}_{\text{0 degree}} + \underbrace{\sum_{q=1}^{M} \sum_{r>q} \mathbb{I}(c_j \in \{q, r\}) s_{j(qr)}(z_{c_j i}) x_{(qr)t}}_{\text{1st degree}} \\ + \underbrace{\sum_{q=1}^{M} \sum_{r>q} \sum_{u>r} \mathbb{I}(c_j \in \{q, r, u\}) s_{j(qru)}(z_{c_j i}) x_{(qru)t} + \cdots}_{\text{2nd degree}} \\ + \underbrace{s_{j(1\ldots M)}(z_{c_j i}) x_{(1\ldots M)t} + \tilde{s}_j(z_{c_j i})}_{\text{(M-1)th degree}} \end{aligned} \tag{8}$$

with $\tilde{s}_j(z_{c_j i}) = 1 - s_{j(q)}(z_{c_j i}) - \sum_{r>q} s_{j(qr)}(z_{c_j i}) - \cdots - s_{j(1\ldots M)}(z_{c_j i}) \in (0, 1)$ and $\boldsymbol{x}_t = [x_{(1)t} \ \cdots \ x_{(M)t} \ x_{(12)t} \ \cdots \ x_{(M-1M)t} \ \cdots \ x_{(1\ldots M)t}]'$. Zero-degree means the absence of compounding effects, whereas $M - 1$ degree means all risks are compounded in a single global risk factor.

3. Inference and posterior approximation

For simplicity and without loss of generality, we discuss the inference for the case of one variable per unit and one common factor. Let us define the collections of observable and latent variables, $\mathbf{r}_{1:T} = (\mathbf{r}_1, \ldots, \mathbf{r}_T)$, $\mathbf{x}_{1:T} = (\mathbf{x}_1, \ldots, \mathbf{x}_T)$ and $\mathbf{v}_{1:T} = (\mathbf{v}_1, \ldots, \mathbf{v}_T)$ and the collection of factor loadings $\lambda = (\lambda_1, \ldots, \lambda_K)$. The complete-data likelihood factorizes as follows $L(\mathbf{r}_{1:T}, \mathbf{x}_{1:T}, \mathbf{v}_{1:T}, \mathbf{z} | \rho, \lambda, \boldsymbol{\pi}) = f(\mathbf{r}_{1:T}, \mathbf{z} | \mathbf{x}_{1:T}, \mathbf{v}_{1:T}, \lambda, \boldsymbol{\pi})$ $h(\mathbf{x}_{1:T}, \mathbf{v}_{1:T} | \rho, d)$, where

$$f(\mathbf{r}_{1:T}, \mathbf{z} | \mathbf{x}_{1:T}, \mathbf{v}_{1:T}, \lambda, \boldsymbol{\pi}) = \left(\prod_{i=1}^{N} \prod_{k=1}^{K} \pi_k^{\mathbb{I}(z_i = k)} \prod_{t=1}^{T} f(r_{it} | x_t, z_i, \lambda) \right) \tag{9}$$

$$h(\mathbf{x}_{1:T}, \mathbf{v}_{1:T} | \rho, d) = \left(\prod_{t=1}^{T} f(x_t | x_{t-1}, \rho, v_t) f(v_t | d) \right). \tag{10}$$

Under the standard quadratic loss function assumption, the estimators of the latent variables and the parameters are their posterior means. The joint posterior distribution is not tractable, nevertheless it can be easily approximated by a Gibbs sampler procedure (Robert et al., 2007; Robert and Casella, 2010), which draws iteratively random samples from the following conditional distributions: (i) sample $\mathbf{z}$ from $p(\mathbf{z} | \mathbf{r}_{1:T}, \mathbf{x}_{1:T}, \lambda, \boldsymbol{\pi})$, (ii) sample $\boldsymbol{\pi}$ from $p(\boldsymbol{\pi} | \mathbf{z})$, (iii) sample λ from $p(\lambda | \mathbf{r}_{1:T}, \mathbf{z}, \mathbf{x}_{1:T})$, (iv) sample $\mathbf{x}_{1:T}$ from $p(\mathbf{x}_{1:T} | \mathbf{v}_{1:T}, \mathbf{r}_{1:T}, \mathbf{z}, \rho)$, (v) sample $\mathbf{v}_{1:T}$ from $p(\mathbf{v}_{1:T} | \mathbf{x}_{1:T}, \rho, d)$ and (vi) sample ρ and d from $p(\rho, d | \mathbf{v}_{1:T}, \mathbf{x}_{1:T})$. The derivation of the full conditional distributions is in Appendix B.

Random draws in steps (i) and (ii) can be obtained exactly, whereas steps from (iii) to (vi) need an approximated sampling method. We applied an adaptive Metropolis–Hastings for both steps. In particular, the scale of the proposal is adapted at each iteration to keep a target acceptance probability of 0.44 (e.g., Łatuszyński et al., 2013). In the case of $\mathbf{x}_{1:T}$ and $\mathbf{v}_{1:T}$ a random block strategy is followed. The total number of blocks remains constant, with the size and composition of each block being randomly selected in every iteration (see for example Chib and

Table 1
COVOL parameter estimates for the absence of compounding specification. Top panels: parameter estimates, 90% credible intervals (in brackets), and Deviance Information Criterion (DIC) and relationships for the two-cluster model (left) and the one-cluster model (right). Middle panel: VAR coefficients between the COVOL factors. Bottom panels: correlations between the COVOL factors.

(a) 6-cluster analysis

	EMI	EUI	GPR
ρ	0.18 [0.1,0.27]	0.11 [0.04,0.22]	0.09 [0.03,0.17]
V	0.68 [0.45,0.94]	1.56 [1.07,2.17]	2.15 [1.71,2.68]
λ_L	0.62 [0.16,0.75]	0.52 [0.43,0.61]	0.73 [0.39,0.77]
λ_H	0.74 [0.62,0.92]	0.88 [0.8,0.94]	0.95 [0.85,0.97]
DIC	54 823.55	12 312.40	10 470.46
	EMI	EUI	GPR
EMI			
EUI	−0.01 [−0.09,0.07]		
GPR	0.05 [−0.01,0.13]	0 [−0.07,0.08]	

(b) 3-cluster analysis

	EMI	EUI	GPR
ρ	0.2 [0.12,0.28]	0.08 [0.04,0.17]	0.09 [0.04,0.18]
V	0.71 [0.47,1.02]	1.05 [0.65,1.5]	1.72 [1.32,2.21]
λ	0.67 [0.58,0.79]	0.71 [0.63,0.82]	0.84 [0.81,0.88]
DIC	54 998.31	12 480.70	10 726.59
	EMI	EUI	GPR
EMI			
EUI	−0.01 [−0.08,0.08]		
GPR	0.06 [−0.01,0.13]	0.01 [−0.06,0.09]	

Ramamurthy, 2010). Members within a block must be adjacent in the time dimension, and single-member blocks are permissible.

The efficiency of the sampler has been studied through some simulation experiments in different settings, which are consistent with the real-data settings of our paper: (i) high persistence in the latent COVOL process; (ii) low persistence in the COVOL process (see Fig. C.9). We reported in Table C.2 of the Appendix the convergence diagnostics of the MCMC for the COVOL and exposure parameters, which includes the Mean Square Error (MSE), the Adjusted Rand Index (ARI), and the Autocorrelation Function (ACF). The results show that the inference procedure and the posterior approximation effectively recover the true value of the latent variable and the parameters (see the ARI and the MSE in the first and third row of Table C.2). The autocorrelation values indicate some dependence in the MCMC draws (see the second row, ACF), which is stronger in the high-persistence setting. Thus, in addition to the burning sample removal, we apply thinning with a rate of 120 for the high- and low-persistence settings.

4. Energy markets and political risk

A preliminary analysis of the data is presented, which includes some stylized facts such as cross-country comovements in the volatility-proxy of the series. Then, the results of the clustered stochastic COVOL model are presented.

4.1. Data description

Following a multi-country perspective, we considered a dataset with 26 countries and excluding those countries with more than 50% of missing observations, which returns a dataset with fifteen countries: Australia, Belgium, Brazil, Canada, China, Germany, France, India, Italy, Japan, Netherlands, South Korea, Spain, United Kingdom and the United States.

For the country i, we define with $y_{i1t} = y_{it}^{(EMI)}$ as the performances of the energy sector, measured by the log-returns of the MSCI Investable Market Index (EMI) for the energy industry. The data were obtained from Refinitiv and Bloomberg to ensure comprehensive coverage, as data for certain countries were available in one provider but missing in the other. The $y_{it}^{(EMI)}$ was constructed by predicting the missing values through a simple regression analysis, which includes log-returns as the dependent variable from Definitive and the log-returns from Bloomberg. After combining the two sources, only 0.58% of the panel data was missing, which was imputed using the country median This proxy of the energy market naturally exhibits volatility clustering effects since it is a stock market variable. We expect country volatilities to be driven by common volatility movements, the EMI-COVOL, and the common volatility to correlate with global uncertainty and risk. In this paper we focus on uncertainty and geopolitical risks and denote with $y_{i2t} = y_{it}^{(EUI)}$ the first difference logarithm of the Energy-Related Uncertainty Index (Dang et al., 2023), and with $y_{i3t} = y_{it}^{(GPR)}$ the first difference logarithm of the Geopolitical Risk Index (Caldara and Iacoviello, 2022). The GPR index is derived using a text-search analysis applied to a predefined set of newspapers, identifying adverse events such as acts and threats at the country level, including war, peace, nuclear activities, military actions, and terrorism. Similarly, the EUI is constructed using a textual approach applied to the reports of the Economist Intelligence Unit, focusing on energy-related keywords and demonstrating a prompt response to oil shocks.[3] For $y_{it}^{(EUI)}$ and $y_{it}^{(GPR)}$, there are no missing observations. The analysis spans from January 2010 to September 2022, corresponding to the common availability of the data at a monthly frequency.[4] It is important to emphasize the high kurtosis and significant asymmetry observed in nearly all variables and countries (see Table D.3), which coexist with a pairwise correlation between their squared values (see Fig. 1). These characteristics suggest potential co-movements that could significantly affect the normality of the variables by influencing the tails and symmetry of their distributions.

We standardized the variables as follows: $r_{it}^{(q)} = (y_{it}^{(q)} - \mathbf{z}_t^{(q)'}\boldsymbol{\beta}_q)/\sigma_{it}^{(q)}$ with $q \in \{EMI, EUI, GPR\}$, where the volatility $\sigma_{it}^{(q)}$ follows a GARCH(1,1) and $\mathbf{z}_t^{(q)}$ is a set of factors common to the variables in the qth block. Following Campos-Martins and Hendry (2024), the common factors are extracted by using PCA. We assume the element of the cross-sectional partitions are $D_{kq} \subset \{1, \ldots, 15\}$ with three variable types, i.e. $q \in \{EMI, EUI, GPR\}$, and two groups within each variable type, that is $k = 1, 2$. The choice of two groups seems reasonable following the preliminary analysis results (see Section 1). Based on our multiple factor COVOL in Section 2.3, three specifications are applied to the energy market and political risk framework: absence of compounding, global compounding, and conditional global compounding. For the global compounding and conditional global compounding specifications, two robustness checks are presented: the inclusion of Russia (for the sample from 2009–06 to 2022–03) and the inclusion of a fourth variable capturing the aggregate stock market returns measured by the log-returns of the MSCI Investable Market Index of all economic sectors (for the sample from 2010–01 to 2022–09).

4.2. Individual risk results

The estimated individual risk COVOLs are in Figs. 4–5. The estimation uncertainty is quantified through the 90% posterior credible

[3] The GPR data were obtained from Matteo Iacoviello's website, while the EUI data were downloaded from policyuncertainty.com.

[4] The individual EMI-COVOL in Section 4.2 is estimated at a weekly frequency, as the three risk variables are independently estimated and therefore analyzed at the lowest frequency available to the authors.

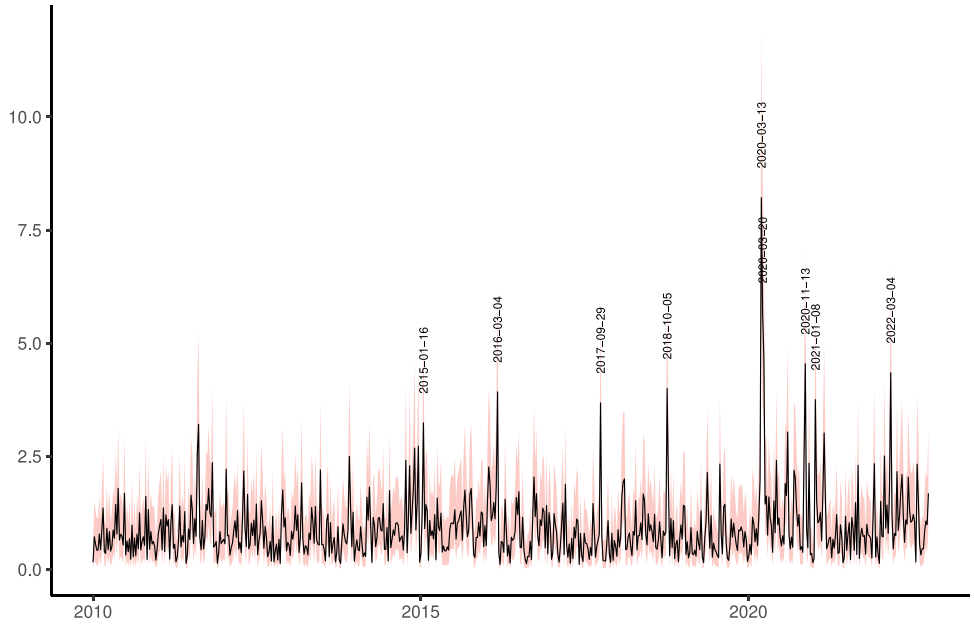

Fig. 4. Estimated Energy Sector common volatility, EMI-COVOL (black line) and its 90% credible interval (shaded area). Labels report the dates of some global financial, economic, and geopolitical events.

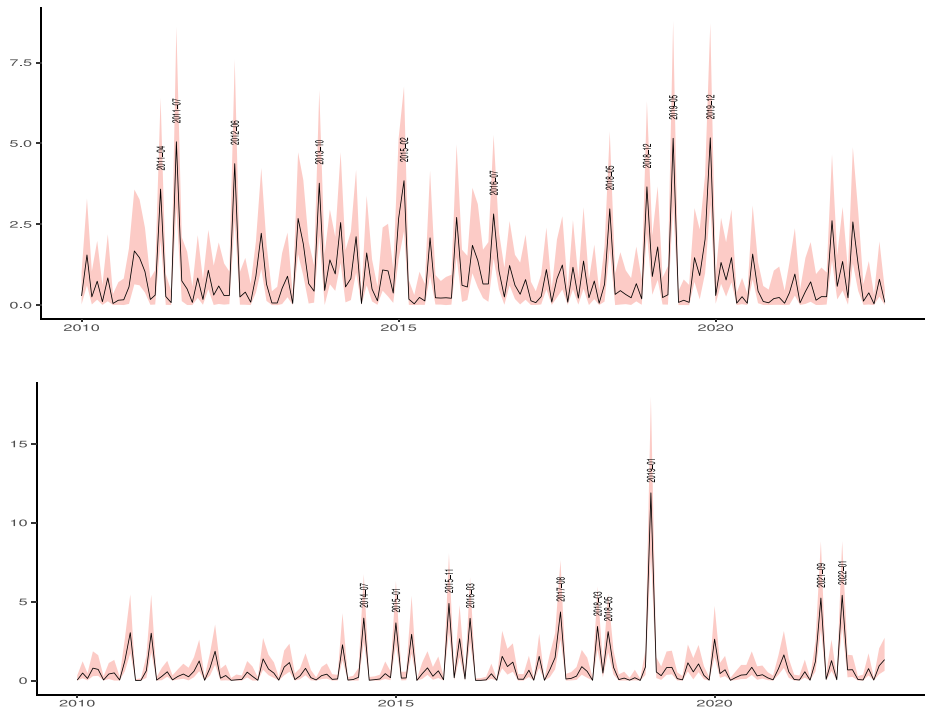

Fig. 5. Estimated Energy Uncertainty (top, EUI-COVOL) and Geopolitical Risk (bottom, GPR-COVOL) common volatility. In each plot: COVOL estimate (black line) and its 90% credible interval (shaded area). Labels report the dates of some global financial, economic, and geopolitical events.

intervals, represented by the shaded areas in the figures. We found evidence of temporal and cross-sectional clustering effects in the stochastic COVOL model without compounding risks.

The three COVOLs peak at the occurrence of major global events (date labels in the figures) and the latent dynamic factor can be used to assess the impact and persistence of a shock during a given period in the following periods. The most pronounced peak in EMI-COVOL occurred in March 2020, coinciding with the COVID-19 outbreak, followed by the second highest peak in November 2020, when a rebound reached its highest level since March 2020.

The EUI-COVOL exhibited two peaks during the first and second quarters of 2011 following the Fukushima nuclear accident, which caused additional global demand for liquefied natural gas (LNG) (Hayashi and Hughes, 2013). The largest subsequent peaks occurred in May 2019, coinciding with both the intensification of the trade barrier

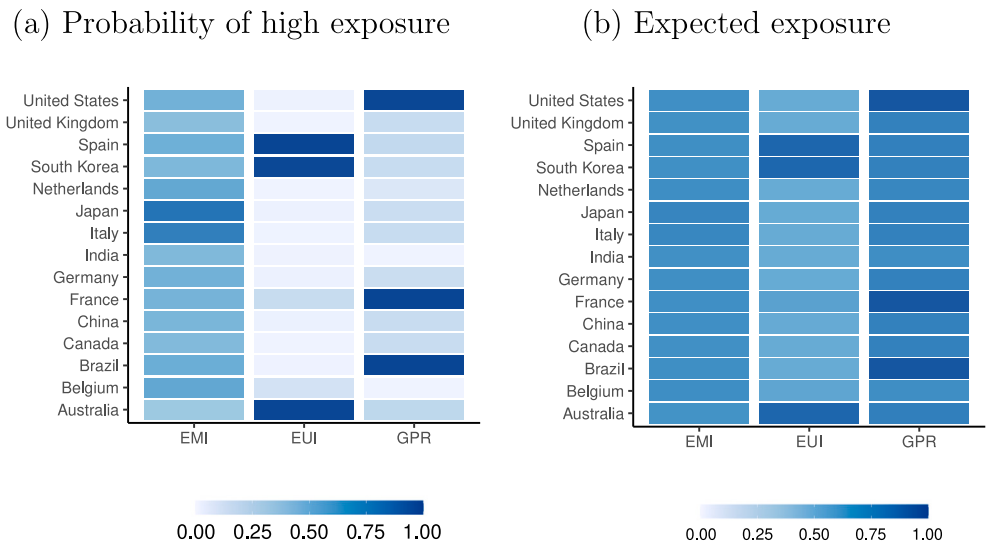

Fig. 6. Countries and variables exposure to the COVOLs in the specification without compounding. Left: probability of high exposure. Right: expected exposure.

between the US and China and with China importing zero US LNG.[5] The GPR-COVOL reached its highest peak in January 2019, coinciding with US sanctions on Venezuelan oil firms, which led to an increase in oil prices.[6]

The three COVOLs began to rise to different degrees with the outbreak of the Russian-Ukrainian conflict. The most pronounced peaks occurred in March 2022 for the EMI-COVOL and subsequently to the Russian invasion of Ukraine. In this respect, the natural gas price in Amsterdam increased to approximately 126 EUR/MWh and soared to an all-time high in August 2022, reaching approximately 240 EUR/MWh.

Our modeling framework can be used to measure the persistence of COVOL. We find evidence of a similar degree of persistence in COVOLs (see the top panel in Table 1). In the 6-cluster analysis (left panel), the energy market co-movements are slightly more persistent ($\rho = 0.18$) compared to the uncertainty ($\rho = 0.11$) and geopolitical co-movements ($\rho = 0.09$), implying a greater predictability of the impact of EMI. Persistence was similar in the 3-cluster analysis (right panel). The results confirm the similar findings obtained by Balli et al. (2022) in a forecasting error variance decomposition framework (Diebold and Yilmaz, 2012). The authors provided evidence of substantial GPR transmission across countries.

Parameter V represents the scale of the COVOL, and large values of V correspond to larger fourth-order moment values of the returns, that is, to fatter return tails (see the results in Propositions 2 and 3). GPR and EUI have larger scales, $V = 2.15$ and $V = 1.56$, respectively, implying that larger GPR or EUI shocks have a higher probability than financial shocks (Engle and Campos-Martins, 2023). This result is robust to the choice of the number of clusters for the GPR (compare panels (a) and (b) in Table 1).

Regarding the exposure and the cross-sectional clustering, we found evidence of different exposure levels to COVOLs across asset clusters and variable types (see λ_L and λ_H estimates in Table 1). Since the credible intervals for the EUI and GPR loadings do not overlap, there is evidence of different exposure levels for the two groups of countries. Regarding the EUI the most exposed countries are Spain, South Korea, and Australia (see panel (a) in Fig. 6). A possible explanation for the differing trends in energy consumption. For instance, Spain and South Korea are importers of natural gas, while Australia exports 74% of its natural gas production.[7] The United States, France, and Brazil are the most exposed to the GPR-COVOL, which could reflect their interdependence on the global markets. The United States and France are the world's first and third-largest exporters, respectively, while Brazil's raw materials constitute a significant share of its exports.[8]

Finally, to compare the model with six clusters ($K = 2$, $M = 3$) against a model with no clusters within variable types ($K = 1$, $M = 3$), we calculate the Deviance Information Criterion (DIC) for each alternative as shown in Table 1. The full model DICs for the models with 6 and 3 clusters are 77 606.40 and 78 205.60, respectively. The results suggest that assuming two clusters per variable type is preferred over assuming a pooled exposure. Indeed, decomposing the full model DIC by variable type indicates that the conclusion holds for EMI, EUI, and GPR, consistently with the preliminary analysis in Fig. 1.

The extraction of common factors for each risk source allowed us to conduct a preliminary compounding risk analysis. Examining the third panel of Table 1, we observe the absence of correlation between the stochastic COVOLs, which suggests the three COVOLs capture distinct sources of risk and uncertainty.

4.3. Compounding risk results

The estimated COVOLs for the two compounding risk specifications, global compounding and conditional global compounding, are presented in Fig. 7. These estimates are provided for three different samples: (i) the standard sample, used in Section 4.2, with fifteen countries and three variables—EMI, EUI, and GPR (black solid line); (ii) an extended sample that adds Russia, shifting the coverage period from 2009–06 to 2022–03 while maintaining the three variables EMI, EUI, and GPR (blue dashed line)[9]; and (iii) a sample of 15 countries (excluding Russia), including EMI, EUI, GPR, and stock market returns as a fourth variable (green dotted line). Considering their similarity, we

[5] See, for example, https://www.cfr.org/timeline/us-china-relations and https://www.energypolicy.columbia.edu/what-chinas-retaliatory-tariff-means-for-us-china-lng-trade/.

[6] Additional information can be retrieved at https://br.usembassy.gov/29299/ and https://www.cnbc.com/2019/01/29/oil-markets-us-sanctions-on-venezuela-in-focus.html.

[7] Source: Australian Government - Geoscience Australia, available at https://www.ga.gov.au/digital-publication/aecr2022/gas.

[8] Source: WorldBank, available at https://wits.worldbank.org/CountryProfile/en/Country/WLD/Year/2019/TradeFlow/EXPIMP/Partner/all and https://wits.worldbank.org/CountrySnapshot/en/BRA/textview.

[9] Although its inclusion does not significantly alter the COVOL estimates over the entire period under investigation, an interesting case emerges with an extraordinary peak in 2022, corresponding to the Russian invasion of Ukraine.

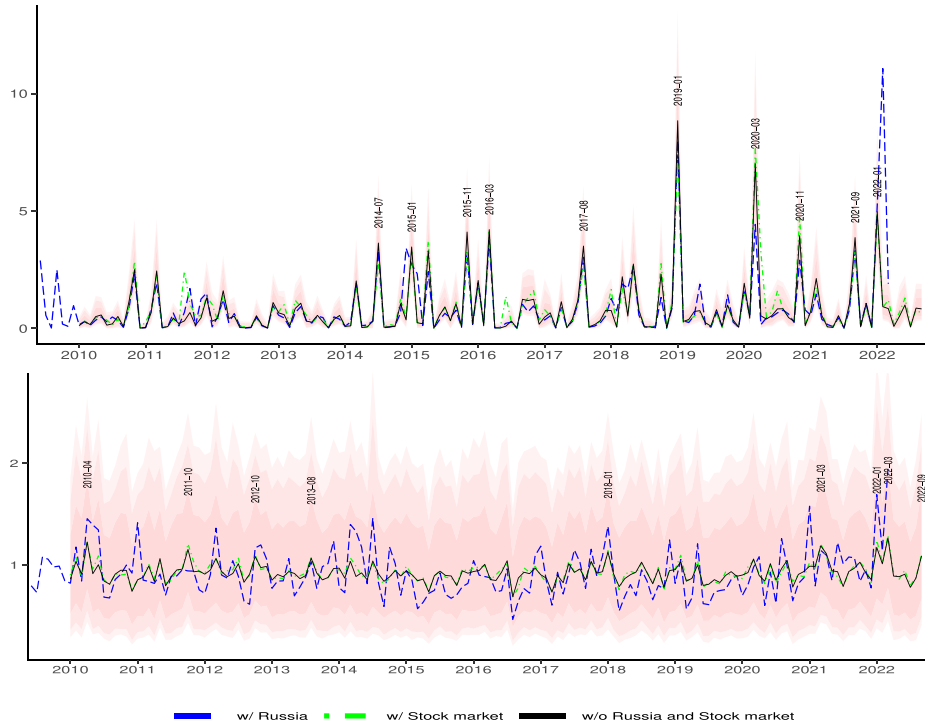

Fig. 7. Estimated Global common volatility, Global-COVOL, and the 70%, 90%, and 95% credible intervals (shaded areas) for the sample without Russia and the stock market (black line) under the global (top) and conditional global (bottom) compounding specifications. The blue dashed line (green dotted line) indicates the results for the sample with Russia (stock market). Labels report the dates of some global financial, economic, and geopolitical events.

first focused our analysis on the results of the standard sample (black solid line).

The top and bottom plots show the results for the Global Compounding and the Conditional Global Compounding, respectively. The two COVOLs exhibit persistence. In the first specification, the estimated autoregressive parameter is $\rho = 0.09$ (see Table D.4) and the most exposed variables are EMI and GPR for all countries (top plots of Fig. 8), which indicates they are the main drivers of the volatility comovements at the global level. Nevertheless, the low expected exposure of EUI calls for using multiple-factor COVOL models. In this analysis, we apply the Conditional Global COVOL specification, which accounts for missing factors by compounding the individual risks.

A feature of the Conditional Global COVOL model is its ability to capture two sources of risks additional to the individual risk models: the global compounding risk $x_{(123)t}$ and the residual exposure $\tilde{s}_j$, which is the complement of the relative importance of all COVOLs. Other proposed models do not address the ability to capture the compounding effect arising from the interactions between the risk factors. In this specification, the estimated global COVOL has a similar persistence ($\rho = 0.19$, see Table D.5 in Appendix), and the risks compounded are mainly EMI of all countries, EUI of Belgium, the UK and the US and more importantly the GPR of Belgium and India (panel (d) in Fig. 8). The policy implications in such a case are noteworthy. Some countries' significant exposure to the global COVOL underlines the need for compounding risks since individual risk COVOLs alone are not enough to explain comovements. The exposures to the individual risk COVOLs (panel (c) of Fig. 8) are comparable with the exposures in the specification without compounding (panel (b) of Fig. 6). The relative importance of individual risk and global compounding risk COVOLs are reported in panel (b) of Fig. D.11 in Appendix. Regarding the average residual exposure across countries is 13.01% for EMI, 15.84% for EUI and 8.93% for GPR, which shows that the four COVOLs explain most of the country's GPR volatility comovements (panel (b) of Fig. D.11 and Table D.6 in Appendix). For further comparison between the specifications, see Fig. D.10 and Table D.7 in Appendix.

Regarding the results across the three samples: the standard sample, the extended sample with Russia, and the inclusion of the stock market returns, there is a high correlation between the COVOL from the standard sample and the COVOLs from the two extended samples. For the (conditional) global compounding specification the correlation is 0.75 (0.67) when Russia is included and 0.95 (0.95) in the case of the stock market is incorporated. More importantly, the red-shaded areas represent the credible intervals for the standard sample, and they cover most data points of the other two cases—including Russia and the stock market returns. This suggests that COVOL estimates remain stable across different cases (see Fig. D.10 for further comparison). The robustness of the result may be explained by the nature of large fluctuations, which produce enough co-movements in other countries/variables allowing for similar COVOL in sub-samples of the data.

Our modeling framework can enhance the efficiency of investment strategies in the global energy market. In addition to the insights provided by a GARCH modeling framework for hedging strategies (e.g., see Billio et al., 2018), our COVOL model can be used to manage volatility co-movements across multiple assets. For instance, the COVOL adjustment can improve the estimation of the variance–covariance matrix of the assets. Table D.8 provides a comparison of the log-likelihood with two benchmark models: a stochastic volatility model with dependent log-volatility errors (Eisenstat et al., 2016) and a constant correlation GARCH (Bollerslev, 1990). The constant correlation GARCH is directly related to the multi-factor COVOL because they are equivalent in the absence of co-movements. The stochastic volatility model represents an alternative approach to measuring risk dependence through a second-order moment. The results suggest that global COVOL performs better than the constant correlation GARCH and is similar to the dependent stochastic volatility model. Still, the conditional global specification performs better than the dependent stochastic volatility and the other benchmark models. To measure the economic value of the fitting improvement, we investigate the models' ability to generate extra returns. A buy-and-hold strategy is implemented based on a repeated Markowitz

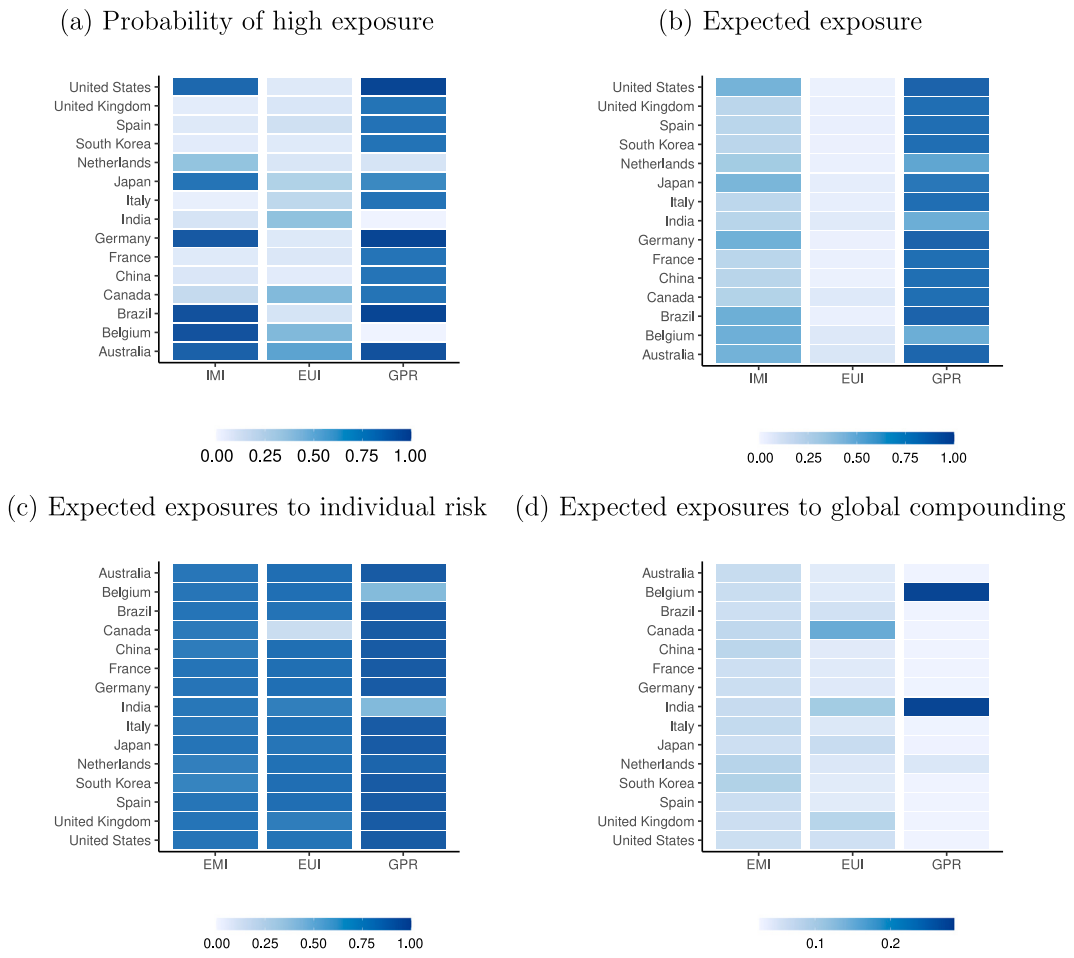

Fig. 8. Compounding risks: Countries (rows) and variable (columns) exposure to the COVOLs. Top: Global Compounding. Bottom: Residual Global Compounding. (For interpretation of the references to color in this figure legend, the reader is referred to the web version of this article.)

portfolio allocation with no short-selling constraints. Fig. D.12 displays the results for various variance–covariance models, including the conditional global COVOL, GARCH, and Global COVOL approaches. Panel (a) shows that the Sharpe ratio–return curve of the conditional global COVOL dominates the other model for expected returns higher than 0.7%. This result aligns with the cumulative Sharpe ratio in panel (b), where expected returns of 1% (4%) yield a Sharpe ratio of 0.855 (1.667) by the end of the period.[10]

Additionally, the conditional global COVOL can be used to implement more refined portfolio strategies, as in Engle and Campos-Martins (2023), where an investor can set a constraint on the maximum exposure to the COVOL factor. In asset allocation, an exposure constraint can be activated at the global or individual levels since the multi-factor COVOL model allows for identifying dependence between alternative sources of risk and uncertainty and their compounding effects.

The heterogeneity in the country's exposure to individual and global COVOLs is valuable information for policymakers aiming at the stability of the energy and financial markets and for the risk management of companies operating in the global markets. The findings suggest that uniform policy responses or risk management decisions based on individual energy risks may not be optimal, implying that decision-makers can benefit from considering the interplay of alternative sources of risks.

[10] We are indebted to an anonymous reviewer for the suggestion on both applications.

5. Conclusion

We study the relationship between the energy sector, energy uncertainty, and geopolitical risk through the lens of a new stochastic multiple common volatility (COVOL) model. We build on COVOL literature and propose a new multivariate model with stochastic COVOL latent factors to investigate the dynamic features of volatility co-movements in a panel of series. Clustered effects in the cross sections are assumed to achieve model parsimony and to capture similarities in the exposure to common factors. We provide evidence of different persistence levels in the COVOL factors across types of variables and exposure levels to the common volatility factors. Thus, our model offers the possibility of forecasting co-movements and supporting macro-prudential policy to stabilize the economic and financial systems. Moreover, we found evidence of risk compounding, characterized by lagged spill-over cross-effects between energy uncertainty, geopolitical risk, and energy sector volatility. A comparison with alternative standard models, such as multivariate GARCH and SV, shows that multi-factor COVOL not only exhibits better fitting but can also be used to improve the performance of financial investment strategies.

CRediT authorship contribution statement

Ovielt Baltodano López: Writing – review & editing, Writing – original draft, Visualization, Validation, Supervision, Software, Resources, Project administration, Methodology, Investigation, Funding acquisition, Formal analysis, Data curation, Conceptualization. **Monica**

Billio: Writing – review & editing, Writing – original draft, Visualization, Validation, Supervision, Software, Resources, Project administration, Methodology, Investigation, Funding acquisition, Formal analysis, Data curation, Conceptualization. **Roberto Casarin:** Writing – review & editing, Writing – original draft, Visualization, Validation, Supervision, Software, Resources, Project administration, Methodology, Investigation, Funding acquisition, Formal analysis, Data curation, Conceptualization. **Michele Costola:** Writing – review & editing, Writing – original draft, Visualization, Validation, Supervision, Software, Resources, Project administration, Methodology, Investigation, Funding acquisition, Formal analysis, Data curation, Conceptualization.

Acknowledgments

The authors acknowledge the support from the European Union - Next Generation EU - '*GRINS - Growing Resilient, INclusive and Sustainable*' project (PE0000018), National Recovery and Resilience Plan (NRRP) - PE9 - Mission 4. RC was supported by the MUR – PRIN project '*Discrete random structures for Bayesian learning and prediction*' under g.a. n. 2022CLTYP4. The views and opinions expressed are only those of the authors and do not necessarily reflect those of the European Union or the European Commission. Neither the European Union nor the European Commission can be held responsible for them. MC also acknowledges research support from the Leibniz Institute for Financial Research SAFE. This research used the HPC multiprocessor cluster system and is part of the Venice Center for Economics and Risk Analytics (VERA) at Ca' Foscari University of Venice. We are grateful to the Editor, Richard S. J. Tol, the special-issue editors, Susana Campos Martins and Tony Klein, and to the two anonymous reviewers for their insightful comments, which helped improve earlier drafts of the manuscript.

Appendix A. Further theoretical results

Proposition 6 (*Conditional Model Properties Given the Membership*). *Let* $(\lambda_1,\dots,\lambda_N)'|\xi \sim \mathcal{D}(\xi_1,\dots,\xi_N)$ *and* $\xi_i \sim \sum_{k=1}^K \pi_k m_k$. *The return process* r_{it} $i=1,\dots,N$ *satisfies*

1. $\mathbb{E}(r_{it}|\mathcal{F}^r_{t-1}\vee\{z_i=k\})=0$ *and* $\mathbb{V}(r_{it}|z_i=k)=1$;
2. $\mathbb{C}ov(r_{it},r_{jt}|\mathcal{F}^r_{t-1}\vee\{z_i=k,z_j=\ell\})=0$;
3. $\mathbb{V}(r^2_{it}|\mathcal{Z})=\frac{3d^2m_k(1+m_k)}{\sum_k N_k m_k(1+\sum_k N_k m_k)}+2$ *where* $z_i=k$;
4. $\mathbb{C}ov(r^2_{it},r^2_{jt}|\mathcal{Z})=\frac{d^2m_km_\ell}{(\sum_k N_k m_k)(1+\sum_k N_k m_k)}$ *where* $z_i=k$ *and* $z_j=\ell$.

Proposition 7 (*Conditional Model Properties with Membership Uncertainty*). *Let* $(\lambda_1,\dots,\lambda_N)'|\xi \sim \mathcal{D}(\xi_1,\dots,\xi_N)$ *and* $\xi_i \sim \sum_{k=1}^K \pi_k m_k$. *The return process* r_{it} $i=1,\dots,N$ *satisfies*

1. $\mathbb{E}(r_{it}|\mathcal{F}_{t-1})=0$ *and* $\mathbb{V}(r_{it}|\mathcal{F}^v_t)=1$;
2. $\mathbb{C}ov(r_{it},r_{jt}|\mathcal{F}_{t-1})=0$;
3. $\mathbb{V}(r^2_{it}|\mathcal{F}^v_t)=3\mathbb{E}\left(\frac{\xi_i(1+\xi_i)}{\xi_0(1+\xi_0)}\right)\left((1-\rho^2)\sum_{s=0}^{t-1}\rho^{2s}v_{t-s}\right)+2$;
4. $\mathbb{C}ov(r^2_{it},r^2_{jt}|\mathcal{F}^v_t)=\mathbb{E}\left(\frac{\xi_i\xi_j}{\xi_0^2}\right)((1-\rho^2)\sum_{s=0}^{t-1}\rho^{2s}v_{t-s})$ *for* $i\neq j$.

Proposition 8 (*Model Properties*). *Let* $(\lambda_1,\dots,\lambda_N)'|\xi \sim \mathcal{D}(\xi_1,\dots,\xi_N)$ *and* $\xi_i \sim \sum_{k=1}^K \pi_k m_k$. *The return process* r_{it} $i=1,\dots,N$ *satisfies*

1. $\mathbb{E}(r_{it})=0$ *and* $\mathbb{V}(r_{it})=1$;
2. $\mathbb{C}ov(r_{it},r_{jt})=0$;
3. $\mathbb{V}(r^2_{it})=3d^2\mathbb{E}\left(\frac{\xi_i(1+\xi_i)}{\xi_0(1+\xi_0)}\right)+2$;
4. $\mathbb{C}ov(r^2_{it},r^2_{jt})=d^2\mathbb{E}\left(\frac{\xi_i\xi_j}{\xi_0^2}\right)$.

Appendix B. Proof of the results in the paper

Proof of Proposition 1.

1. The conditional mean of the latent COVOL process is $\mathbb{E}\left(x_t|\mathcal{F}^v_t\right)=\mathbb{E}\left(\mathbb{E}\left(x_t|x_{t-1},\mathcal{F}^v_t\right)|\mathcal{F}^v_t\right)=(1-\rho)(1+\rho+\cdots+\rho^{t-1})+\rho^t\mathbb{E}\left(x_0\right)=1$ and the unconditional mean is $\mathbb{E}\left(x_t\right)=\mathbb{E}\left(\mathbb{E}\left(x_t|\mathcal{F}^v_t\right)\right)=1$
2. The conditional variance is
$$\begin{aligned}&\mathbb{V}\left(x_t|\mathcal{F}^v_t\right)=\mathbb{V}\left(\mathbb{E}\left(x_t|x_{t-1},\mathcal{F}^v_t\right)\right)+\mathbb{E}\left(\mathbb{V}\left(x_t|x_{t-1},\mathcal{F}^v_t\right)|\mathcal{F}^v_t\right)\\&=\mathbb{V}\left((1-\rho)+\rho x_{t-1}|\mathcal{F}^v_t\right)+\mathbb{E}\left((1-\rho)v_t((1-\rho)+2\rho x_{t-1})|\mathcal{F}^v_t\right)\\&=\rho^2\mathbb{V}\left(x_{t-1}|\mathcal{F}^v_t\right)+(1-\rho^2)v_t=(1-\rho^2)\sum_{i=0}^{t-1}\rho^{2i}v_{t-i}.\end{aligned}$$
The unconditional variance is
$$\mathbb{V}\left(x_t\right)=\mathbb{V}\left(\mathbb{E}\left(x_t|\mathcal{F}^v_t\right)\right)+\mathbb{E}\left(\mathbb{V}\left(x_t|\mathcal{F}^v_t\right)\right)=\mathbb{E}\left((1-\rho^2)\sum_{i=0}^{t-1}\rho^{2i}v_{t-i}\right)=d^2$$
3. The conditional and unconditional autocovariances of the latent COVOL process at the hth lag are
$$\begin{aligned}&\mathbb{C}ov(x_t,x_{t-h}|\mathcal{F}^v_t)=\mathbb{E}(x_tx_{t-h}|\mathcal{F}^v_t)-1=\mathbb{E}(x_{t-h}\mathbb{E}(x_t|\mathcal{F}^x_{t-1},\mathcal{F}^v_t)|\mathcal{F}^v_t)-1\\&=(1-\rho)+\rho\mathbb{E}(x_{t-h}x_{t-1}|\mathcal{F}^v_t)-1=(1-\rho)(1+\rho+\cdots+\rho^{h-1})\\&\quad+\rho^h\mathbb{E}(x^2_{t-h}|\mathcal{F}^v_t)-1\\&=(1-\rho^h)-(1-\rho^h)+\rho^h(1-\rho^2)\sum_{i=0}^{t-h-1}\rho^{2i}v_{t-i}\\&=\rho^h(1-\rho^2)\sum_{i=0}^{t-h-1}\rho^{2i}v_{t-i}\\&\mathbb{C}ov(x_t,x_{t-h})=\mathbb{E}(\mathbb{C}ov(x_t,x_{t-h}|\mathcal{F}^v_t))=\rho^hd^2.\end{aligned}$$

Proof of Proposition 2.

1. The conditional mean and variance of the observable process given the membership allocation variable are
$$\begin{aligned}&\mathbb{E}(r_{it}|\mathcal{F}^r_{t-1}\vee\{z_i=k\})=\mathbb{E}(\sqrt{g_i(x_t)}|\mathcal{F}^r_{t-1}\vee\{z_i=k\})\mathbb{E}(\varepsilon_{it})=0\\&\mathbb{V}(r_{it}|z_i=k)=\mathbb{E}(r^2_{it}|\vee\{z_i=k\})=(s(z_i)\mathbb{E}(x_t)+1-s(z_i))\mathbb{E}(\varepsilon^2_{it})=1\end{aligned}$$
2. The conditional covariance of the observable process given the group membership is
$$\begin{aligned}&\mathbb{C}ov(r_{it},r_{jt}|\mathcal{F}^r_{t-1}\vee\{z_i=k,z_j=\ell\})\\&=\mathbb{E}(r_{it}r_{jt}|\mathcal{F}^r_{t-1}\vee\{z_i=k,z_j=\ell\})\\&=\mathbb{E}(\sqrt{g_i(x_t)}\sqrt{g_j(x_t)}|\mathcal{F}^r_{t-1}\vee\{z_i=k,z_j=\ell\})\mathbb{E}(\varepsilon_{it}\varepsilon_{jt})=0\end{aligned}$$
3. The conditional variance of the square of the observable process given the group membership is
$$\begin{aligned}&\mathbb{V}(r^2_{it}|z_i=k)=\mathbb{E}(r^4_{it}|z_i=k)-1=\mathbb{E}(\varepsilon^4_{it})\\&\times\mathbb{E}([s(z_i)x_t+1-s(z_i)]^2|z_i=k)-1\\&=3(\lambda_k^2\mathbb{E}(x_t^2)-\lambda_k^2+1)-1=3\lambda_k^2d^2+2\end{aligned}$$
4. The conditional covariance of the square of the observable process given the group membership is
$$\begin{aligned}&\mathbb{C}ov(r^2_{it},r^2_{jt}|z_i=k,z_j=\ell)=\mathbb{E}(r^2_{it}r^2_{jt}|z_i=k,z_j=\ell)-1\\&=\mathbb{E}(\varepsilon^2_{it})\mathbb{E}(\varepsilon^2_{jt})\mathbb{E}([s(z_i)x_t+1-s(z_i)]\\&\times[s(z_j)x_t+1-s(z_j)]|z_i=k,z_j=\ell)-1\\&=\lambda_k\lambda_\ell\mathbb{E}(x_t^2)+1-\lambda_k\lambda_\ell-1=d^2\lambda_k\lambda_\ell\end{aligned}$$

Proof of Proposition 3.

1. The conditional mean and variance of the observable process are
$$\mathbb{E}(r_{it}|\mathcal{F}_{t-1})=\mathbb{E}(\sqrt{g_i(x_t)}|\mathcal{F}_{t-1})\mathbb{E}(\varepsilon_{it})=0$$

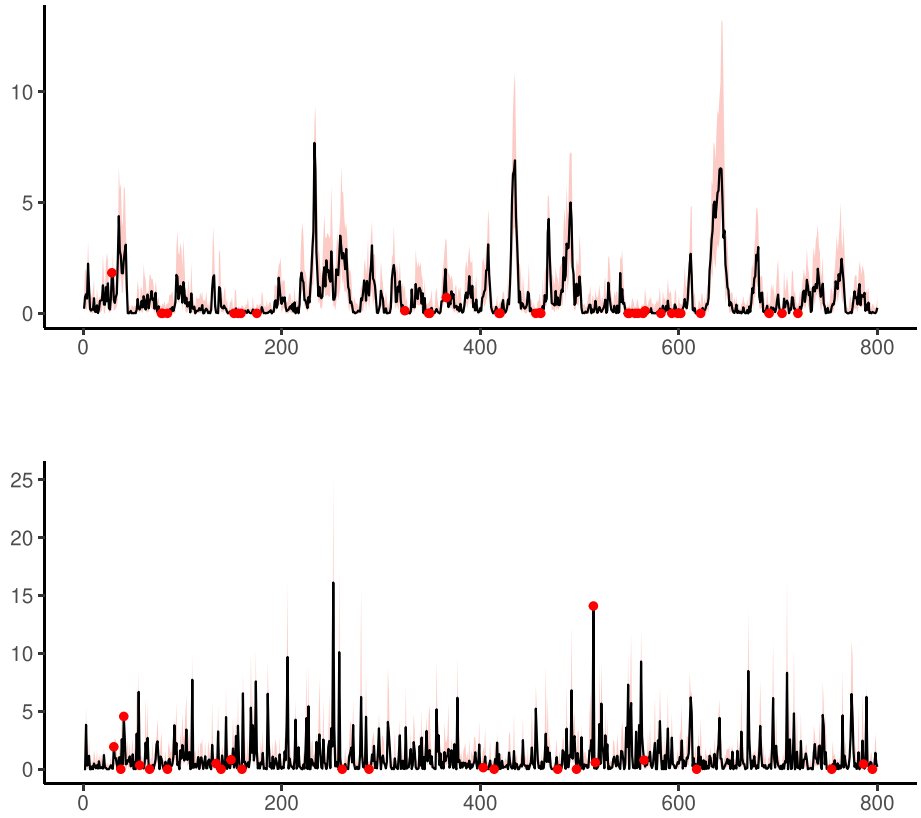

Fig. C.9. Latent COVOL dynamics in a high-persistence ($\rho = 0.9$, top plot) and low-persistence ($\rho = 0.1$, bottom plot) setting.

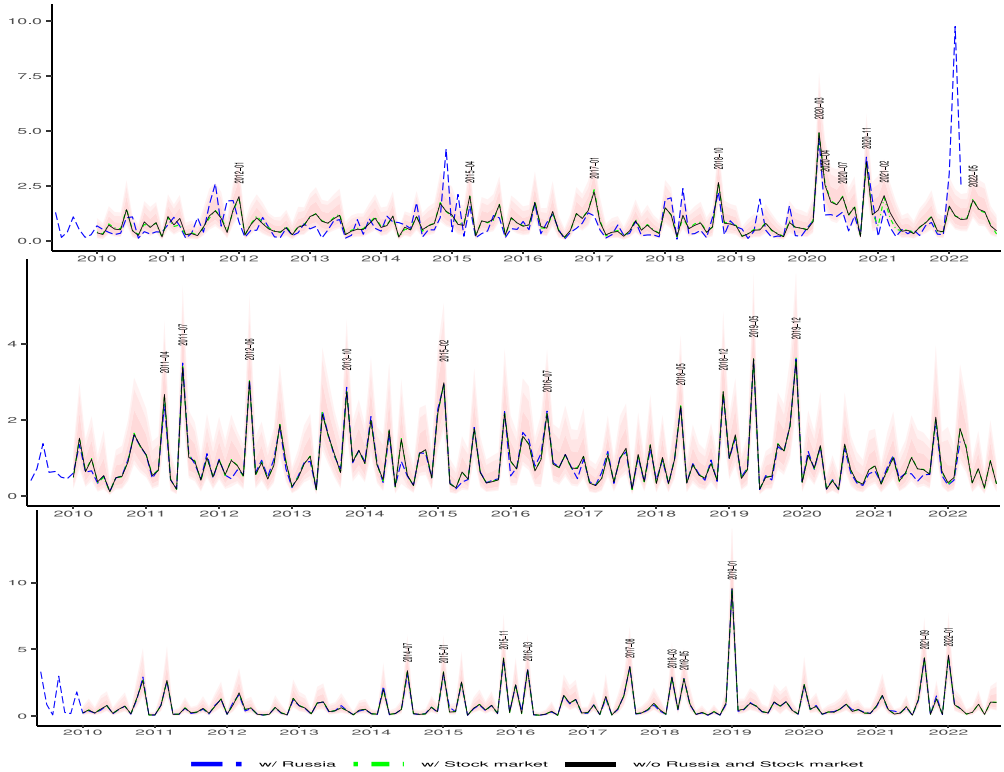

Fig. D.10. Conditional Global compounding specification: Estimated common volatility for the Energy Sector,EMI-COVOL (top panel), Energy uncertainty, EUI-COVOL (middle panel), and the Global political index, GPR-COVOL (bottom panel), and the 70%, 90% and 95% credible interval (shaded areas) for the sample without Russia and the stock market (black line). The blue dashed (green dotted) line indicates the results for the sample with Russia (the stock market). Labels report the dates of some global financial, economic, and geopolitical events.

Table C.2
Simulation results: Accuracy (measured by Mean Square Error and Adjusted Rand Index) and efficiency (assessed by first–lag autocorrelation) of the MCMC sampler for different persistence levels (ρ), before and after thinning.

Performance	Parameter	Before thinning		After thinning	
		$\rho = 0.9$	$\rho = 0.1$	$\rho = 0.9$	$\rho = 0.1$
ARI	z	1.0000(0.0000)	1.0000(0.0000)		
	π	−9e−04(0.0031)	4e−04(0.0033)	−8e−04(0.0146)	−0.0052(0.0143)
	ρ	0.9572(0.0047)	0.6874(0.0198)	0.4739(0.0422)	0.0193(0.0188)
ACF	V	0.8755(0.0157)	0.7711(0.0199)	0.5122(0.0486)	0.4043(0.0538)
	λ	0.9351(0.0107)	0.9194(0.0084)	0.4847(0.0488)	0.3927(0.0266)
	x	0.8723(0.0069)	0.8949(0.0037)	0.1948(0.0288)	0.2629(0.0190)
	π	0.0147(0.0000)	0.0049(0.0000)	7e−04(0.0000)	2e−04(0.0000)
	ρ	0.0018(0.0010)	0.0026(0.0021)	1e−04(1e−04)	1e−04(1e−04)
MSE	V	0.0900(0.0642)	0.0433(0.0358)	0.0045(0.0032)	0.0022(0.0018)
	λ	2e−04(1e−04)	2e−04(1e−04)	0.0000(0.0000)	0.0000(0.0000)
	x	0.2758(0.1074)	0.4167(0.0503)	0.0138(0.0054)	0.0208(0.0025)

Note: Mean Square Error (MSE), the Adjusted Rand Index (ARI), and the Autocorrelation at the first lag ($ACF(1)$).

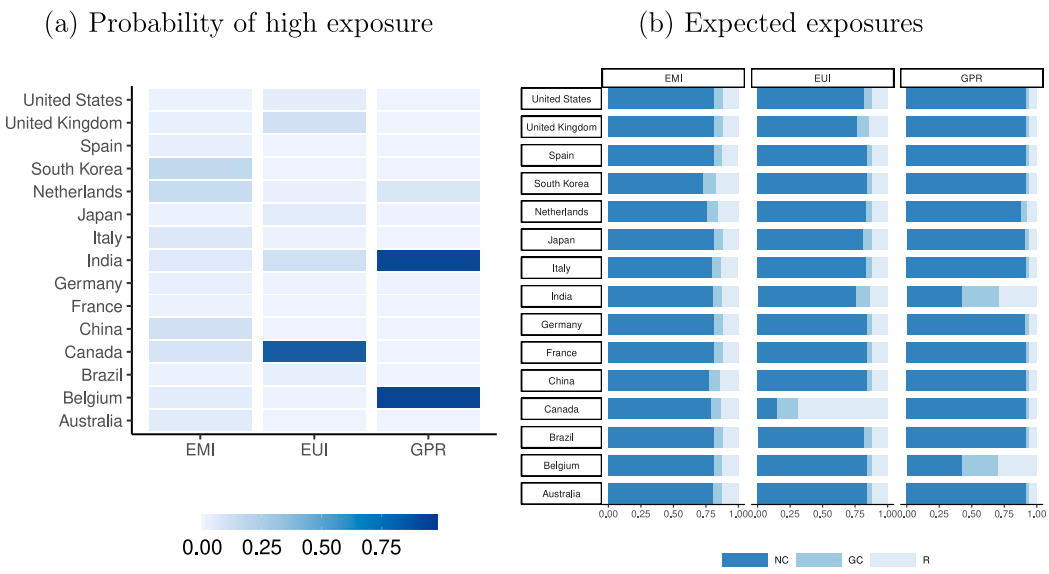

Fig. D.11. Countries exposure to the COVOLs for the conditional Global compounding specification. Left: probability of high exposure to global compounding. Right: Expected exposure to individual risk (NC), global factor (GR), and the unexplained component (R).

$$\mathbb{V}(r_{it}|\mathcal{F}_t^v) = \mathbb{E}(r_{it}^2|\mathcal{F}_t^v) = \mathbb{E}[s(z_i)\mathbb{E}(x_t|\mathcal{F}_t^v \vee \{z=k\}) + 1 - s(z_i)|\mathcal{F}_t^v]\mathbb{E}(\varepsilon_{it}^2) = 1$$

2. The conditional covariance of the observable process is

$$\mathbb{C}ov(r_{it}, r_{jt}|\mathcal{F}_{t-1}) = \mathbb{E}(r_{it}r_{jt}|\mathcal{F}_{t-1}) = \mathbb{E}(\sqrt{g_i(x_t)}\sqrt{g_j(x_t)}|\mathcal{F}_{t-1})\mathbb{E}(\varepsilon_{it}\varepsilon_{jt}) = 0$$

3. The conditional variance of the square of the observable process is

$$\mathbb{V}(r_{it}^2|\mathcal{F}_t^v) = \mathbb{E}(r_{it}^4|\mathcal{F}_t^v) - 1 = \mathbb{E}(\varepsilon_{it}^4)\mathbb{E}([s(z_i)x_t + 1 - s(z_i)]^2|\mathcal{F}_t^v) - 1$$
$$= 3(\mathbb{E}(s(z_i)^2)\mathbb{E}(x_t^2|\mathcal{F}_t^v) + \mathbb{E}(s(z_i)^2) + 1) - 1$$
$$= 3[(1-\rho^2)\sum_{s=0}^{t-1}\rho^{2s}v_{t-s}][\sum_k\sum_\ell \pi_k\pi_\ell\lambda_k\lambda_\ell] + 2$$

4. The conditional covariance of the square of the observable process is

$$\mathbb{C}ov(r_{it}^2, r_{jt}^2|\mathcal{F}_t^v) = \mathbb{E}(r_{it}^2, r_{jt}^2|\mathcal{F}_t^v) - 1$$
$$= \mathbb{E}(\varepsilon_{it}^2)\mathbb{E}(\varepsilon_{jt}^2)\mathbb{E}([s(z_i)x_t + 1 - s(z_i)][s(z_j)x_t + 1 - s(z_j)]|\mathcal{F}_t^v) - 1$$
$$= \mathbb{E}(s(z_i)s(z_j))\mathbb{E}(x_t^2) + 1 - \mathbb{E}(s(z_i)s(z_j)) - 1$$
$$= [(1-\rho^2)\sum_{s=0}^{t-1}\rho^{2s}v_{t-s}]\sum_{k=1}^{K}\sum_{\ell=1}^{K}\lambda_k\lambda_\ell\pi_k\pi_\ell$$

Proof of Proposition 4.

1. The conditional serial autocorrelation of the square of the observable process is

$$\mathbb{C}ov(r_{it}^2, r_{jt-h}^2|\mathcal{F}_t^v) = \mathbb{E}(r_{it}^2, r_{jt-h}^2|\mathcal{F}_t^v) - 1$$
$$= \mathbb{E}(\varepsilon_{it}^2)\mathbb{E}(\varepsilon_{jt-h}^2)\mathbb{E}([s(z_i)x_t + 1 - s(z_i)][s(z_j)x_{t-h} + 1 - s(z_j)]|\mathcal{F}_t^v) - 1$$
$$= \mathbb{E}(s(z_i)s(z_j))\mathbb{E}(x_t x_{t-h}|\mathcal{F}_t^v) + 1 - \mathbb{E}(s(z_i)s(z_j)) - 1$$
$$= \rho^h(1-\rho^2)(\sum_{s=0}^{t-h-1}\rho^{2s}v_{t-s})(\sum_k\sum_\ell \pi_k\pi_\ell\lambda_k\lambda_\ell)$$

2. The unconditional serial autocorrelation of the square of the observable process is

$$\mathbb{C}ov(r_{it}^2, r_{jt-h}^2) = \mathbb{E}(\mathbb{C}ov(r_{it}^2, r_{jt-h}^2|\mathcal{F}_t^v)) = \rho^h d^2\sum_k\sum_\ell \pi_k\pi_\ell\lambda_k\lambda_\ell$$

3. The conditional serial autocorrelation of the square of the observable process given the memberships is

$$\mathbb{C}ov(r_{it}^2, r_{jt-h}^2|z_i=k, z_j=\ell) = \mathbb{E}(r_{it}^2, r_{jt-h}^2|z_i=k, z_j=\ell) - 1$$
$$= \mathbb{E}(\varepsilon_{it}^2)\mathbb{E}(\varepsilon_{jt-h}^2)\mathbb{E}([s(z_i)x_t + 1 - s(z_i)] \times [s(z_j)x_{t-h} + 1 - s(z_j)]|z_i=k, z_j=\ell) - 1$$
$$= \lambda_k\lambda_\ell\mathbb{E}(x_t x_{t-h}) + 1 - \lambda_k\lambda_\ell - 1 = \rho^h d^2\lambda_k\lambda_\ell$$

Table D.3
Empirical moments and the p-value of the Jarque–Bera test for EMI, EUI, and GPR in percentage scale.

Country	Mean	Variance	Kurtosis	Skewness	JB
EMI					
Australia	−0.03	12.36	9.46	−0.75	0
Belgium	0.16	21.93	4.95	0.12	0
Brazil	−0.01	37.26	6.99	0.08	0
Canada	0.02	9.22	12.58	−1.16	0
China	0.01	12.36	4.06	−0.07	0
France	0.07	13.24	15.88	−0.13	0
Germany	0.44	32.52	8.35	−0.44	0
India	0.18	10.05	5.14	−0.11	0
Italy	−0.02	13.86	12.54	−0.92	0
Japan	0.01	8.58	6.42	−0.47	0
Netherlands	−0.04	13.65	6.1	−0.35	0
South Korea	0.15	20.47	10.54	1	0
Spain	0.09	19.48	6.64	0.06	0
United Kingdom	0.05	13.41	13.33	−0.34	0
United States	0.1	13.12	8.66	−0.59	0
EUI					
Australia	15.39	4739.72	13.27	2.6	0
Belgium	16.26	5019.47	12.09	2.46	0
Brazil	10.91	2779.69	5.86	1.44	0
Canada	9.93	2432.92	5.97	1.46	0
China	15.83	4644.55	11	2.12	0
France	11.79	3306.31	10.95	2.23	0
Germany	11.38	3116.3	8.26	1.94	0
India	14.54	4078.85	5.94	1.57	0
Italy	12.89	3411.34	9.36	1.96	0
Japan	13.24	3562.66	8.02	1.76	0
Netherlands	13.34	3942.72	11.04	2.16	0
South Korea	10.95	3340.36	9.51	2.14	0
Spain	16.63	5098.51	9.06	2.18	0
United Kingdom	6.11	1386.11	8.51	1.72	0
United States	15.93	4636.34	9.71	1.98	0
GPR					
Australia	25.66	9893.83	13.88	2.82	0
Belgium	19.94	5578.85	5.92	1.53	0
Brazil	40.59	22 994.4	26.67	4.07	0
Canada	13.06	4027.34	10.81	2.31	0
China	8.51	1984.89	6.53	1.48	0
France	13.19	5995.5	33.75	4.88	0
Germany	10.46	2551.4	7.12	1.56	0
India	12.62	3492.32	6.99	1.69	0
Italy	17.6	5294.13	7.9	1.91	0
Japan	17.32	4997.48	5.11	1.48	0
Netherlands	20.81	7209.63	11.31	2.31	0
South Korea	12.66	3812.03	14.09	2.62	0
Spain	22.35	8559.23	12.68	2.7	0
United Kingdom	4.7	1039.51	6.84	1.38	0
United States	2.95	614.02	5.51	1.07	0

Table D.4
COVOL persistence and scale parameter estimates and the clusters' exposures for the global compounding specification. Parameter estimates, 90% credible intervals (in brackets).

	Common	EMI	EUI	GPR
ρ	0.09 [0.03,0.18]			
V	1.83 [1.44,2.34]			
λ_L		0.2 [0.09,0.31]	0.01 [0,0.05]	0.47 [0.33,0.74]
λ_H		0.51 [0.38,0.62]	0.12 [0.02,0.27]	0.88 [0.84,0.95]

Table D.5
COVOL persistence and scale parameter estimates for the conditional global compounding specification. Parameter estimates, 90% credible intervals (in brackets).

	EMI	EUI	GPR	Global
ρ	0.22 [0.1,0.38]	0.09 [0.04,0.19]	0.08 [0.03,0.17]	0.18 [0.07,0.37]
V	0.56 [0.42,0.74]	0.62 [0.48,0.82]	1.19 [0.98,1.44]	0.22 [0.11,0.39]

Table D.6
Clusters' exposures estimates for the conditional global compounding specification. Parameter estimates, 90% credible intervals (in brackets). NC: Individual risk COVOL, GC: Global compounding risk COVOL and R: Unexplained component.

Group	NC	GC	R
EMI			
λ_L	0.82 [0.74,0.89]	0.06 [0.02,0.12]	0.12 [0.07,0.18]
λ_H	0.3 [0.03,0.65]	0.29 [0.08,0.62]	0.33 [0.15,0.79]
EUI			
λ_L	0.84 [0.78,0.9]	0.04 [0.02,0.08]	0.11 [0.07,0.17]
λ_H	0.04 [0.01,0.36]	0.08 [0.03,0.66]	0.89 [0.15,0.95]
GPR			
λ_L	0.92 [0.89,0.94]	0.02 [0.01,0.05]	0.06 [0.04,0.08]
λ_H	0.42 [0.22,0.57]	0.28 [0.1,0.49]	0.28 [0.15,0.5]

Proof of Proposition 5.

1. The unconditional mean and variance of the observable process are

$$\mathbb{E}(r_{it}) = \mathbb{E}(\mathbb{E}(r_{it}|\mathcal{F}^r_{t-1} \vee \{z_i = k\})) = 0$$
$$\mathbb{V}(r_{it}) = \mathbb{E}(\mathbb{V}(r_{it}|z_i = k)) = 1$$

2. The unconditional covariance of the observable process is

$$\mathbb{C}ov(r_{it}, r_{jt}) = \mathbb{E}(\mathbb{C}ov(r_{it}, r_{jt}|\mathcal{F}^r_{t-1} \vee \{z_i = k, z_j = \ell\})) = 0$$

3. The unconditional variance of the square of the observable process is

$$\mathbb{V}(r^2_{it}) = \mathbb{E}(\mathbb{V}(r^2_{it}|z_i = k)) = 3d^2(\sum_k \sum_\ell \pi_k \pi_\ell \lambda_k \lambda_\ell) + 2$$

4. The unconditional covariance of the square of the observable process is

$$\mathbb{C}ov(r^2_{it}, r^2_{jt}) = \mathbb{E}(\mathbb{C}ov(r^2_{it}, r^2_{jt}|z_i = k, z_j = \ell)) = d^2 \sum_{k=1}^K \sum_{\ell=1}^K \lambda_k \lambda_\ell \pi_k \pi_\ell$$

Proof of Proposition 6.

1. The conditional mean and variance of the observable process given the membership are

$$\mathbb{E}(r_{it}|\mathcal{F}^r_{t-1} \vee \{z_i = k\}) = \mathbb{E}(\sqrt{g_i(x_t)}|\mathcal{F}^r_{t-1} \vee \{z_i = k\})\mathbb{E}(\varepsilon_{it}) = 0$$
$$\mathbb{V}(r_{it}|z_i = k) = \mathbb{E}(r^2_{it}| \vee \{z_i = k\}) = (\lambda_i \mathbb{E}(x_t) + 1 - \lambda_i)\mathbb{E}(\varepsilon^2_{it}) = 1$$

2. The conditional covariance of the observable process is

$$\begin{aligned}&\mathbb{C}ov(r_{it}, r_{jt}|\mathcal{F}^r_{t-1} \vee \{z_i = k, z_j = \ell\})\\ &= \mathbb{E}(r_{it} r_{jt}|\mathcal{F}^r_{t-1} \vee \{z_i = k, z_j = \ell\})\\ &= \mathbb{E}(\sqrt{g_i(x_t)}\sqrt{g_j(x_t)}|\mathcal{F}^r_{t-1} \vee \{z_i = k, z_j = \ell\})\mathbb{E}(\varepsilon_{it}\varepsilon_{jt}) = 0\end{aligned}$$

3. The conditional variance of the square of the observable process is

$$\begin{aligned}&\mathbb{V}(r^2_{it}|\mathcal{Z}) = \mathbb{E}(r^4_{it}|\mathcal{Z}) - 1 = \mathbb{E}(\varepsilon^4_{it})\mathbb{E}([\lambda_i x_t + 1 - \lambda_i]^2|\mathcal{Z}) - 1\\ &= 3(\mathbb{E}(\lambda^2_i|\mathcal{Z})\mathbb{E}(x^2_t) - \mathbb{E}(\lambda^2_i|\mathcal{Z}) + 1) - 1\\ &= 3d^2\mathbb{E}(\mathbb{V}(\lambda_i|\mathcal{Z}, \xi) + \mathbb{E}(\lambda_i|\mathcal{Z}, \xi)^2|\mathcal{Z}) + 2\\ &= \frac{3d^2 m_k(1 + m_k)}{\sum_k N_k m_k(1 + \sum_k N_k m_k)} + 2\end{aligned}$$

4. The conditional covariance of the square of the observable process is

$$\mathbb{C}ov(r^2_{it}, r^2_{jt}|\mathcal{Z}) = \mathbb{E}(r^2_{it}, r^2_{jt}|\mathcal{Z}) - 1$$

Table D.7
Correlations between COVOLs under the different model specifications: Conditional Global compounding, Absence of compounding and Global compounding. EMI, EUI, GPR and GC correspond to the individual COVOLs for financial returns in the energy sector, energy uncertainty and geopolitical risk and the second degree compounding risk, respectively.

	RGC				AC			GC
	EMI	EUI	GPR	GC	EMI	EUI	GPR	GC
EMI								
EUI	−0.09 [−0.17,−0.01]							
GPR	0.04 [−0.03,0.12]	0 [−0.08,0.09]						
GC	0 [−0.13,0.15]	−0.01 [−0.13,0.12]	0.02 [−0.1,0.17]					
EMI	0.59 [0.49,0.68]	−0.02 [−0.09,0.06]	0.05 [−0.01,0.13]	0.05 [−0.08,0.21]				
EUI	−0.09 [−0.16,−0.01]	0.73 [0.66,0.8]	0 [−0.07,0.08]	0.01 [−0.11,0.16]	−0.01 [−0.09,0.07]			
GPR	0.03 [−0.04,0.11]	0 [−0.07,0.09]	0.88 [0.81,0.92]	0.04 [−0.08,0.19]	0.05 [−0.01,0.13]	0 [−0.07,0.08]		
GC	0.36 [0.25,0.48]	−0.02 [−0.09,0.07]	0.76 [0.67,0.83]	0.05 [−0.08,0.21]	0.39 [0.28,0.51]	−0.01 [−0.08,0.08]	0.76 [0.66,0.84]	

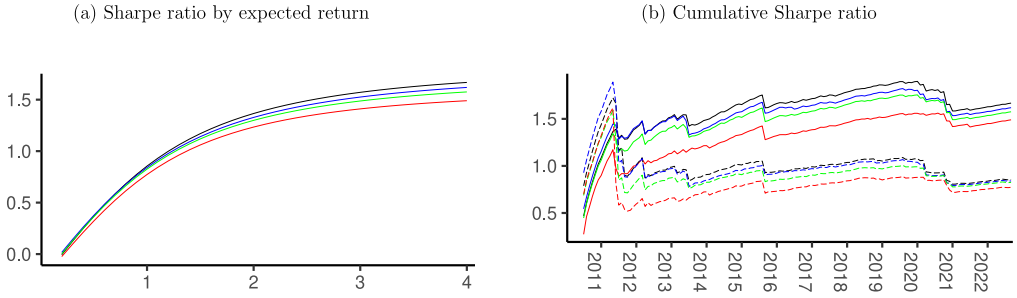

Fig. D.12. Portfolio results for conditional global COVOL (black), GARCH (blue), global COVOL (green), and stochastic volatility (red). The left panel shows the Sharpe ratio (y-axis) for a range of expected returns from 0.1% to 4% (x-axis). The right panel displays the cumulative Sharpe ratio (y-axis) for expected returns of 1% (dashed) and 4% (solid) for the period 2010–2022 (x-axis). (For interpretation of the references to color in this figure legend, the reader is referred to the web version of this article.)

Table D.8
Log-likelihood comparison for multivariate variance models.

Model	Log-likelihood
Constant correlation GARCH (Bollerslev, 1990)	−22 321.30
Dependent Stochastic volatility (Eisenstat et al., 2016)	−21 538.85
Global specification of stochastic COVOL	−21 664.11
Conditional global specification of stochastic COVOL	−21 235.05

$$= \mathbb{E}(\varepsilon_{it}^2)\mathbb{E}(\varepsilon_{jt}^2)\mathbb{E}([s(z_i)x_t + 1 - s(z_i)][s(z_j)x_t + 1 - s(z_j)]|\mathcal{Z}) - 1$$
$$= \mathbb{E}(\lambda_i\lambda_j|\mathcal{Z})\mathbb{E}(x_t^2) + 1 - \mathbb{E}(\lambda_i\lambda_j|\mathcal{Z}) - 1 = d^2\mathbb{E}\left(\frac{\xi_i\xi_j}{\xi_0(1+\xi_0)}\middle|\mathcal{Z}\right)$$
$$= \frac{d^2 m_k m_\ell}{(\sum_k N_k m_k)(1+\sum_k N_k m_k)}$$

Proof of Proposition 7.

1. The conditional mean and variance of the observable process are
$$\mathbb{E}(r_{it}|\mathcal{F}_{t-1}) = \mathbb{E}(\sqrt{g_i(x_t)}|\mathcal{F}_{t-1})\mathbb{E}(\varepsilon_{it}) = 0$$
$$\mathbb{V}(r_{it}|\mathcal{F}_t^v) = \mathbb{E}(r_{it}^2|\mathcal{F}_t^v) = \mathbb{E}[\lambda_i\mathbb{E}(x_t|\mathcal{F}_t^v \vee \{z = k\}) + 1 - \lambda_i|\mathcal{F}_t^v]$$
$$\times\mathbb{E}(\varepsilon_{it}^2) = 1$$

2. The conditional covariance of the observable process is
$$\mathbb{C}ov(r_{it}, r_{jt}|\mathcal{F}_{t-1}) = \mathbb{E}(r_{it}r_{jt}|\mathcal{F}_{t-1})$$
$$= \mathbb{E}(\sqrt{g_i(x_t)}\sqrt{g_j(x_t)}|\mathcal{F}_{t-1})\mathbb{E}(\varepsilon_{it}\varepsilon_{jt}) = 0$$

3. The conditional variance of the square of the observable process is
$$\mathbb{V}(r_{it}^2|\mathcal{F}_t^v) = \mathbb{E}(r_{it}^4|\mathcal{F}_t^v) - 1 = \mathbb{E}(\varepsilon_{it}^4)\mathbb{E}([\lambda_i x_t + 1 - \lambda_i]^2|\mathcal{F}_t^v) - 1$$
$$= 3(\mathbb{E}(\lambda_i^2)\mathbb{E}(x_t^2|\mathcal{F}_t^v) + \mathbb{E}(\lambda_i^2) + 1) - 1$$
$$= 3\mathbb{E}\left(\frac{\xi_i(1+\xi_i)}{\xi_0(1+\xi_0)}\right)\left((1-\rho^2)\sum_{s=0}^{t-1}\rho^{2s}v_{t-s}\right) + 2$$

4. The conditional covariance of the square of the observable process is
$$\mathbb{C}ov(r_{it}^2, r_{jt}^2|\mathcal{F}_t^v) = \mathbb{E}(r_{it}^2, r_{jt}^2|\mathcal{F}_t^v) - 1$$
$$= \mathbb{E}(\varepsilon_{it}^2)\mathbb{E}(\varepsilon_{jt}^2)\mathbb{E}([\lambda_i x_t + 1 - \lambda_i][\lambda_j x_t + 1 - \lambda_j]|\mathcal{F}_t^v) - 1$$
$$= \mathbb{E}(\lambda_i\lambda_j)\mathbb{E}(x_t^2) + 1 - \mathbb{E}(\lambda_i\lambda_j) - 1$$
$$= \mathbb{E}\left(\frac{\xi_i\xi_j}{\xi_0^2}\right)((1-\rho^2)\sum_{s=0}^{t-1}\rho^{2s}v_{t-s})$$

Proof of Proposition 8.

1. The unconditional mean and variance of the observable process are
$$\mathbb{E}(r_{it}) = \mathbb{E}(\mathbb{E}(r_{it}|\mathcal{F}_{t-1}^r \vee \{z_i = k\})) = 0$$
$$\mathbb{V}(r_{it}) = \mathbb{E}(\mathbb{V}(r_{it}|z_i = k)) = 1$$

2. The unconditional covariance of the observable process is
$$\mathbb{C}ov(r_{it}, r_{jt}) = \mathbb{E}(\mathbb{C}ov(r_{it}, r_{jt}|\mathcal{F}_{t-1}^r \vee \{z_i = k, z_j = \ell\})) = 0$$

3. The unconditional variance of the square of the observable process is
$$\mathbb{V}(r_{it}^2) = \mathbb{E}(\mathbb{V}(r_{it}^2|z_i = k)) = 3d^2\mathbb{E}\left(\frac{\xi_i(1+\xi_i)}{\xi_0(1+\xi_0)}\right) + 2$$

4. The unconditional covariance of the square of the observable process is

$$\mathbb{C}ov(r_{it}^2, r_{jt}^2) = \mathbb{E}(\mathbb{C}ov(r_{it}^2, r_{jt}^2 | z_i = k, z_j = \ell)) = d^2\mathbb{E}\left(\frac{\xi_i\xi_j}{\xi_0^2}\right)$$

Derivation of the full conditional distributions

(i) Full conditional distribution of the group membership variable $\mathbf{z}$

$$p(\mathbf{z}|\mathbf{r}_{1:T}, \mathbf{x}_{1:T}, \lambda, \boldsymbol{\pi}) \propto \prod_{i=1}^{N}\prod_{k=1}^{K}\left(\pi_k \prod_{t=1}^{T} f(r_{it}|x_t, k, \lambda)\right)^{\mathbb{I}(z_i=k)} \tag{B.1}$$

$$\propto \prod_{i=1}^{N} \mathcal{M}(\mathbf{z}|p_{i1}, \dots, p_{iK}), \tag{B.2}$$

where $\mathcal{M}(\cdot|p_{i1}, \dots, p_{iK})$ is a multinoulli distribution with probabilities $p_{ik} = \gamma_{ik}/\sum_{k=1}^{K}\gamma_{ik}$ and

$$\gamma_{ik} = \pi_k \prod_{t=1}^{T} f(r_{it}|x_t, k, \lambda).$$

(ii) Full conditional distribution of the membership probabilities $\boldsymbol{\pi}$

$$p(\boldsymbol{\pi}|\mathbf{z}) \propto \left(\prod_{i=1}^{N}\prod_{k=1}^{K}\pi_k^{\mathbb{I}(z_i=k)}\right)\left(\prod_{k=1}^{K}\pi_k^{1/K-1}\right) \tag{B.3}$$

$$\propto \prod_{k=1}^{K}\pi_k^{N_k+1/K-1} \propto \mathcal{D}(p_1, \dots, p_K), \tag{B.4}$$

where the concentration parameters corresponds to $p_k = N_k + 1/K$ and $N_k = \mathbb{I}(z_1 = k) + \cdots + \mathbb{I}(z_N = k)$.

(iii) Full conditional distribution of COVOL loading coefficients λ

$$p(\lambda|\mathbf{r}_{1:T}, \mathbf{z}, \mathbf{x}_{1:T}) \propto \prod_{k=1}^{K}\mathbb{I}(0 < \lambda_k < 1)\left(\prod_{i=1}^{N}\prod_{t=1}^{T} f(r_{it}|x_t, z_i, \lambda)\right) \tag{B.5}$$

$$\propto \prod_{k=1}^{K}\mathbb{I}(0 < \lambda_k < 1)\prod_{t=1}^{T}\prod_{i\in\mathfrak{I}_k}(\lambda_k x_t + 1 - \lambda_k)^{-1/2}\exp\left(-\frac{r_{it}^2}{2(\lambda_k x_t + 1 - \lambda_k)}\right) \tag{B.6}$$

is not tractable, thus we apply MH, where $\mathfrak{I}_k = \{i : z_i = k\}$.

(iv) Full conditional distribution of the latent COVOL process $\mathbf{x}_{1:T}$

$$p(\mathbf{x}_{1:T}|\mathbf{v}_{1:T}, \mathbf{r}_{1:T}, \mathbf{z}, \rho) \propto \prod_{t=1}^{T}\left(\prod_{i=1}^{N} f(r_{it}|x_t, z_i, \lambda)\right) f(x_t|x_{t-1}, \rho, v_t)$$

$$\propto \prod_{t=1}^{T}\left(\prod_{i=1}^{N} f(r_{it}|x_t, z_i, \lambda)\right)\exp\left(-\frac{x_t}{(1-\rho)v_t}\right)$$

$$\sum_{k=0}^{\infty}\left(\frac{x_t^{1/v_t+k-1}}{((1-\rho)v_t)^{1/v_t+k}\Gamma(1/v_t+k)}\right.$$

$$\left.\times \frac{\exp(-(\rho/((1-\rho)v_t))x_{t-1})((\rho/((1-\rho)v_t))x_{t-1})^k}{k!}\right) \tag{B.7}$$

where $x_0 = 1$. Since the full conditional posterior is not tractable, we apply adaptive MH in a random block scheme. The number of blocks is fixed, and the size of each block and its members are chosen uniformly at random at each iteration (see for example Chib and Ramamurthy, 2010). The members of a block must be neighbors in the time dimension, and blocks with only one member are allowed.

(v) Full conditional distribution of random scaling factor $\mathbf{v}_{1:T}$

$$p(\mathbf{v}_{1:T}|\mathbf{x}_{1:T}, \rho) \propto \prod_{t=1}^{T} f(v_t|d) f(x_t|x_{t-1}, \rho, v_t)$$

$$\propto \prod_{t=1}^{T} f(v_t|d)\exp\left(-\frac{x_t}{(1-\rho)v_t}\right)$$

$$\sum_{k=0}^{\infty}\left(\frac{x_t^{1/v_t+k-1}}{[(1-\rho)v_t]^{1/v_t+k}\Gamma(1/v_t+k)}\right.$$

$$\left.\times \frac{\exp(-(\rho/((1-\rho)v_t))x_{t-1})([\rho/((1-\rho)v_t)]x_{t-1})^k}{k!}\right), \tag{B.8}$$

the posterior of the scale parameters is approximated through an adaptive MH step.

(vi) Full conditional distribution of the persistence parameter ρ

Let $\eta = \text{logit}(\rho) = \log(\rho/(1-\rho))$ and assume a Normal prior on η with prior variance σ_η^2., then the full conditional posterior distribution is

$$p(\eta|\mathbf{v}_{1:T}, \mathbf{x}_{1:T}) \propto h(\eta)\prod_{t=1}^{T} f(x_t|x_{t-1}, \text{logit}^{-1}(\eta), v_t)$$

$$\propto \exp(-\eta^2/\sigma_\eta^2)\prod_{t=1}^{T} f(x_t|x_{t-1}, \text{logit}^{-1}(\eta), v_t), \tag{B.9}$$

which is approximated using an adaptive MH step.

Appendix C. Simulation results

We provide some results of a simulation study of the posterior approximation efficiency. We considered two frequent settings occurring in real-data applications: (i) high persistence in the COVOL and (ii) low persistence in the COVOL.

Fig. C.9 illustrates the actual trajectories (black lines), the estimated trajectories (red lines), and their 99% posterior credible intervals (shade areas) in the two settings. Red dots indicate the actual values that do not belong to the 99% credible interval.

Appendix D. Further empirical results

See Figs. D.10–D.12 and Tables D.3–D.8.

References

Agudze, K.M., Billio, M., Casarin, R., Ravazzolo, F., 2022. Markov switching panel with endogenous synchronization effects. J. Econometrics 230 (2), 281–298.

Aguilar, O., West, M., 2000. Bayesian dynamic factor models and portfolio allocation. J. Bus. Econom. Statist. 18 (3), 338–357.

Ahelegbey, D.F., Billio, M., Casarin, R., 2016a. Bayesian Graphical Models for Structural Vector Autoregressive Processes. J. Appl. Econometrics 31 (2), 357–386.

Ahelegbey, D.F., Billio, M., Casarin, R., 2016b. Sparse graphical vector autoregression: A Bayesian approach. Ann. Econ. Stat./ Ann. Econ. Stat. (123/124), 333–361.

Ahelegbey, D.F., Billio, M., Casarin, R., 2024. Modeling turning points in the global equity market. Econ. Stat. 30, 60–75.

Alitab, D., Bormetti, G., Corsi, F., Majewski, A.A., 2019. A jump and smile ride: Jump and variance risk premia in option pricing. J. Financ. Econ. 18 (1), 121–157.

Bai, J., Ng, S., 2006. Evaluating latent and observed factors in macroeconomics and finance. J. Econometrics 131 (1–2), 507–537.

Baker, S.R., Bloom, N., Davis, S.J., 2016. Measuring economic policy uncertainty. Q. J. Econ. 131 (4), 1593–1636.

Balli, F., Balli, H.O., Hasan, M., Gregory-Allen, R., 2022. Geopolitical risk spillovers and its determinants. Ann. Reg. Sci. 68 (2), 463–500.

Baur, D.G., Smales, L.A., 2020. Hedging geopolitical risk with precious metals. J. Bank. Financ. 117, 105823.

Bauwens, L., Rombouts, J., 2007. Bayesian clustering of many GARCH models. Econometric Rev. 26 (2–4), 365–386.

Biernacki, C., Celeux, G., Govaert, G., 2000. Assessing a mixture model for clustering with the integrated completed likelihood. IEEE Trans. Pattern Anal. Mach. Intell. 22 (7), 719–725.

Billio, M., Casarin, R., Osuntuyi, A., 2018. Markov switching GARCH models for Bayesian hedging on energy futures markets. Energy Econ. 70, 545–562.

Billio, M., Casarin, R., Rossini, L., 2019. Bayesian nonparametric sparse VAR models. J. Econometrics 212 (1), 97–115.

Billio, M., Varotto, S., 2020. A New World Post COVID-19: Lessons for Business, the Finance Industry and Policy Makers. Venezia Edizioni Ca' Foscari–Digital Publishing.

Bollerslev, T., 1990. Modelling the coherence in short-run nominal exchange rates: a multivariate generalized ARCH model. Rev. Econ. Stat. 498–505.

Bormetti, G., Casarin, R., Corsi, F., Livieri, G., 2020. A stochastic volatility model with realized measures for option pricing. J. Bus. Econom. Statist. 38 (4), 856–871.

Caldara, D., Iacoviello, M., 2022. Measuring geopolitical risk. Am. Econ. Rev. 112 (4), 1194–1225.

Campos-Martins, S., Hendry, D.F., 2024. Common volatility shocks driven by the global carbon transition. J. Econometrics 239 (1), 105472.

Casarin, R., Costantini, M., Osuntuyi, A., 2024. Bayesian nonparametric panel Markov-switching GARCH models. J. Bus. Econom. Statist. 42 (1), 135–146.
Chib, S., Ramamurthy, S., 2010. Tailored randomized block MCMC methods with application to DSGE models. J. Econometrics 155 (1), 19–38.
Costola, M., Lorusso, M., 2022. Spillovers among energy commodities and the Russian stock market. J. Commod. Mark. 28, 100249.
Creal, D., Koopman, S.J., Lucas, A., 2013. Generalized autoregressive score models with applications. J. Appl. Econometrics 28 (5), 777–795.
Dang, T.H.-N., Nguyen, C.P., Lee, G.S., Nguyen, B.Q., Le, T.T., 2023. Measuring the energy-related uncertainty index. Energy Econ. 124, 106817.
Diebold, F.X., Yilmaz, K., 2012. Better to give than to receive: Predictive directional measurement of volatility spillovers. Int. J. Forecast. 28 (1), 57–66.
Dunz, N., Essenfelder, A.H., Mazzocchetti, A., Monasterolo, I., Raberto, M., 2023. Compounding COVID-19 and climate risks: The interplay of banks' lending and government's policy in the shock recovery. J. Bank. Financ. 152, 106306.
Egorov, K., 2023. Why did Russian economy not collapse under sanctions: Pre-war evidence. In: SAFE Policy Letter. N. 102.
Eisenstat, E., Chan, J.C., Strachan, R.W., 2016. Stochastic model specification search for time-varying parameter VARs. Econometric Rev. 35 (8–10), 1638–1665.
Engle, R., 2002. New frontiers for ARCH models. J. Appl. Econometrics 17 (5), 425–446.
Engle, R.F., Campos-Martins, S., 2023. What are the events that shake our world? Measuring and hedging global COVOL. J. Financ. Econ. 147 (1), 221–242.
Engle, R.F., Gallo, G.M., 2006. A multiple indicators model for volatility using intra-daily data. J. Econometrics 131 (1–2), 3–27.
Engle, R.F., Russell, J.R., 1998. Autoregressive conditional duration: a new model for irregularly spaced transaction data. Econometrica 1127–1162.
Epstein, L.G., Wang, T., 2004. Intertemporal asset pricing under knightian uncertainty. In: Uncertainty in Economic Theory. Routledge, pp. 445–487.
Fisher, M., Jensen, M.J., 2022. Bayesian nonparametric learning of how skill is distributed across the mutual fund industry. J. Econometrics 230 (1), 131–153.
Gong, X., Xu, J., 2022. Geopolitical risk and dynamic connectedness between commodity markets. Energy Econ. 110, 106028.
Gouriéroux, C., Jasiak, J., 2006. Autoregressive gamma processes. J. Forecast. 25 (2), 129–152.
Gregor Kastner, S.F.-S., Lopes, H.F., 2017. Efficient Bayesian inference for multivariate factor stochastic volatility models. J. Comput. Graph. Statist. 26 (4), 905–917.
Hamilton, J.D., 1983. Oil and the macroeconomy since world war II. J. Political Econ. 91 (2), 228–248.
Han, Y., 2006. Asset allocation with a high dimensional latent factor stochastic volatility model. Rev. Financ. Stud. 19 (1), 237–271.
Hayashi, M., Hughes, L., 2013. The Fukushima nuclear accident and its effect on global energy security. Energy Policy 59, 102–111.
Hirano, K., 2002. Semiparametric Bayesian inference in autoregressive panel data models. Econometrica 70 (2), 781–799.
Knight, F.H., 1921. Risk, Uncertainty and Profit. Vol. 31, Houghton Mifflin.
Kruczkiewicz, A., Klopp, J., Fisher, J., Mason, S., McClain, S., Sheekh, N.M., Moss, R., Parks, R., Braneon, C., 2021. Compound risks and complex emergencies require new approaches to preparedness. Proc. Natl. Acad. Sci. 118 (19), e2106795118.
Łatuszyński, K., Roberts, G.O., Rosenthal, J.S., 2013. Adaptive Gibbs sampler and related MCMC methods. Ann. Appl. Probab. 23 (1), 66–98.
Leger, J.-B., 2016. Blockmodels: A R-package for estimating in latent block model and stochastic block model, with various probability functions, with or without covariates. arXiv preprint arXiv:1602.07587.
Liu, J., Ma, F., Tang, Y., Zhang, Y., 2019. Geopolitical risk and oil volatility: A new insight. Energy Econ. 84, 104548.
Mariadassou, M., Robin, S., Vacher, C., 2010. Uncovering latent structure in valued graphs: a variational approach. Ann. Appl. Stat. 4 (2), 715–742.
Robert, C.P., Casella, G., 2010. Introducing Monte Carlo Methods with R. Vol. 18, Springer.
Robert, C.P., et al., 2007. The Bayesian Choice: From Decision-Theoretic Foundations to Computational Implementation. Vol. 2, Springer.
Smales, L.A., 2021. Geopolitical risk and volatility spillovers in oil and stock markets. Q. Rev. Econ. Financ. 80, 358–366.
Wang, X., Wu, Y., Xu, W., 2019. Geopolitical risk and investment. J. Money Credit. Bank..
Yamauchi, Y., Omori, Y., 2023. Dynamic factor, leverage and realized covariances in multivariate stochastic volatility. Econometric Rev. 42 (6), 513–539.